國立臺灣大學理學院物理研究所

博士論文

Department of Physics
College of Science
National Taiwan University

Doctoral Dissertation

二維拓樸絕緣體元件的量子傳輸

Quantum Transport in 2D Topological Insulator Device

李欣翰
Hsin-Han Lee

指導教授：張慶瑞教授
Advisor: Ching-Ray Chang, Prof.

中華民國 103 年 7 月
July, 2014

國立臺灣大學博士學位論文
口試委員會審定書

二維拓樸絕緣體元件的量子傳輸

Quantum Transport in 2D Topological Insulator Device

本論文係李欣翰君（D98222018）在國立臺灣大學物理學系、所完成之博士學位論文，於民國 103 年 7 月 3 日承下列考試委員審查通過及口試及格，特此證明

口試委員：

（簽名）

（指導教授）

Quantum Transport in 2D Topological Insulator Device

二維拓樸絕緣體元件的量子傳輸

by

Hsin-Han Lee (李欣翰)

B.S.(Tamkang University) 2007
M.S.(National Taiwan Normal University) 2009

A dissertation submitted in partial satisfaction of the
requirements for the degree of
Doctor of Philosophy
in
Physics
in the
GRADUATE DIVISION
of the
NATIONAL TAIWAN UNIVERSITY, TAIPEI

Committee in charge:
Professor Ching-Ray Chang (張慶瑞), Chair
Professor Chong-Der Hu (胡崇德)
Professor Chao-Cheng Kaun (關肇正)
Professor Yeu-Chung Lin (林育中)
Professor Shun-Qing Shen(沈順清)
Professor Son-Hsien Chen (陳松賢)

July 2014

Quantum Transport in 2D Topological Insulator Device

二維拓樸絕緣體元件的量子傳輸

by

Hsin-Han Lee (李欣翰)

To my dear parents—

僅獻給我最親愛的父親，母親—
李森嚴先生與郭蕙芳女士

致謝

博士班五年過去了，學了很多事，認識很多人。對我而言，做研究就像即興演奏，拿著手上的樂器 (研究方法)，遵守固定的格式 (物理定律)，還要蒐集好的樂句 (想法)，重點是 --在還沒開始演奏前永遠不知道自己會怎麼做。

這篇論文的完成要感謝指導教授張慶瑞老師這五年的照顧，張教授的帶領下常常讓我們激發出新的想法，也提供給我五年自由的學術空間，並且包容我粗心的個性，很慶幸選到一位這樣好的指導教授。感謝口試委員胡崇德老師、關肇政老師、林育中老師、沈順清老師及陳松賢老師的指導，這篇論文得以完成。感謝女朋友郁婷，在博士班後兩年的陪伴，給我精神上的鼓勵，讓我在研究期間不會寂寞。感謝研究室的每位學長都會熱情地幫助我解決問題，也從學長們到很多做研究和做人做事的態度。明豪學長強大的自律能力，松賢學長對於知識的熱誠，國瑋學長對事情有獨到的見解，，建良學長對生活的態度，又新學長人際交流實力的強大，銘鍵學長學習的主動。另外也感謝研究室同學的陪伴，跟俊岳同學討論物理學到很多，琮暐同學常常辦活動很嗨，薈如同學在我寫論文期間的幫助，國進學弟常常幫我處理很多事，智豪學弟樸實的幽默，意誠學弟樂觀的態度，柏叡學弟的風趣，博士後 Ivo 熱心幫我修改文章。感謝常來研究室串門子的甫哥的建議。感謝博班第一年同一個研究室同學的陪伴，安良學長、國興同學、士綸同學、雅玲同學，讓我在這年準備資格考期間不會孤單。感謝系辦季先生友善的態度、秘書品穎和意玲的幫忙。感謝淡江口琴社的校友在畢業後仍給我支持與鼓勵。感謝我待過的 Taipei Rocket 88 樂團，這幾個月的團練讓我緊繃的壓力得以紓解。感謝我心靈的夥伴 --口琴。

最後感謝我的家人物質上和精神上的幫助。

07, 18, 2014 李欣翰

中文摘要

量子力學中，電子有一個有別於實空間上的自由度稱為自旋。而電子的自旋會與軌道運動互相影響，我們稱此效應為" 自旋軌道耦合"，在某些材料中此效應非常顯著，甚至可以影響巨觀尺度下的物理性質。而自旋電子學就是在研究這些材料的性質或應用，而拓樸絕緣體為此領域中的新興材料。

近年來，拓樸絕緣體已成為一個很有潛力的研究領域，它有可能是製作新一代自旋電子學元件和量子資訊的材料。在理論方面，量子力學的拓樸學應用有許多階段的研究。拓樸絕緣體的內部性質為一般的絕緣體，但是邊緣（表面）卻是導體，這是由於固體內部的電子能帶結構所決定的二維拓樸絕緣體具有特殊的邊緣（表面）態，這種特殊的量子態是由強自旋軌道耦合下所產生，而它的電導取決於邊緣態的數目。在二為拓樸絕緣體外加電場的情況下，兩個邊緣態上的電流會有相反的自旋，稱為量子自旋霍爾效應。一般認為，沿著邊緣狀態的電子不能被非磁性雜質散射，這是由於時間反演對稱性所導致。

在本論文中，我們考慮兩種對量子自旋霍爾效應影響的作用。首先是幾何形狀的影響，我們計算了兩種分支形狀的拓樸絕緣體的電流和自旋極化。我們的結果發現，分支狀的結構將增強自旋極化電流。第二是非磁性雜質的影響，我們研究非磁性雜質加入拓樸絕緣體的傳輸性質。雖然拓樸絕緣體的時間反演對稱性會保護邊緣態的電子不會被非磁性雜質散射，但邊緣的電子會穿隧到另一側的邊緣，導致電子的穿透係數下降。對於雜質的小樣本，傳輸係數甚至可以下降到零。最後，考慮分叉結構和雜質所構成的元件中，我們發現了電子同時擁有量子穿隧和量子干涉的效應，而這兩種效應會影響電子的傳輸方向。從這些結果推得此結構可以成為一種電子元件，藉由閘電位控制電流的開關，且具有自旋性質。以上這些性質皆是由 Landauer formula 進行數值研究。

關鍵詞：拓樸絕緣體、量子自旋霍爾效應、自旋軌道耦合、量子傳輸、格林函數、鋸齒型邊界二維蜂巢晶格帶、碲化汞─碲化鎘量子井

Abstract

In quantum mechanics, the electrons have a degree of freedom is different from the real space is called spin. In some situations, the electron spin and orbital motion affect each other, this important effect is spin-orbit coupling, in some materials this effect is very significant and can even affect the physical properties of macroscopic scale. The spintronics is a research in the nature or application of these materials, and Topological Insulator is a novel material in this field.

Recently, topological insulator is an emerged field in condensed matter physics and material science; it has been regarded as the materials which have potential applicate in the new generation of spintronics devices and quantum computer. For the theory, there are many phase and topology studies in the quantum mechanics in this topic. The topological insulator is the material that is insulating in the bulk but conducting on the edge (or surface). In two dimension, it exhibits the quantum spin Hall effect. The effect is caused by the strong spin-orbit coupling and the spin Hall conductance is determined by the number of edge state. It is believed that electron transport along the edge states cannot be backscattered by the non-magnetic impurity due to the time reversal symmetry.

In the thesis, we study the transport property of quantum spin Hall effect in defined geometries and effect caused by the impurities. First, we calculated the current and polarization on two types of branching topological insulators. Our results indicate that the branch structure will enhance the spin polarizing

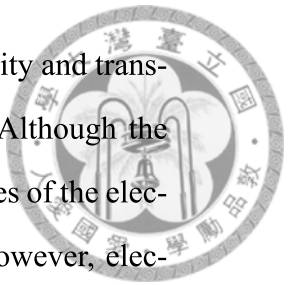

current. Second, the influences of impurity on the electron density and transmission of a finite topological insulator sample are studied. Although the time-reversal symmetry topology insulators will protect the edges of the electronic states cannot be scattering by non-magnetic impurity, however, electrons from one side can tunnel into the other side and the quantized conductance can be broken down. For a small sample with impurity, the transmission coefficient can even drop to zero for the crosswalk between the helical edge states at two sample sides. At last, a device is designed based in those two influences. We found that quantum tunneling and quantum interference occur in the same time, and both effects influence the direction of the electron. Those properties are studied numerically in the framework of Landauer Formalism.

Keywords: topological insulator, quantum spin Hall effect, spin-orbit coupling, quantum transport, Green function, zigzag honeycomb nano-ribbon, HgTe/CdTe quantum well

Contents

List of Publication

[1] **Hsin-Han Lee** and Ching-Ray Chang, *Spin transport calculation for the branchshaped zigzag graphene nanoribbon*, J. Appl. Phys. 111, 07C521 (2012).

[2] **Hsin-Han Lee** and Ching-Ray Chang, *Impurity influence in quantum spin Hall transport*, Phys. Rev. B 88, 195149 (2013).

List of Figures

Chapter 1

Introduction

1.1 Overview

For a long time, people are try to found new generation devices as an information storage, transmission and processing are carried out using spin current and spin accumulation, which are controlled with electric field or voltage. The spintronics make the idea possible implement that by induce the addition dimensional "spin".

Now, there is a novel material has been found that is the insulator in the bulk state but the conductance in the edge state (or surface state in three dimension), we call that "Topological Insulator". Actually, in a topological insulator, the surface state is not an ordinary metal. However, the direction and spin of the surface electrons are locked together by the time reversal symmetry. And in the general situation, the most surprising prediction is that the surface electrons cannot be scattered by defects or other perturbations and thus meet little or no resistance as they travel. That means the states remain "topologically protected" they cannot scatter without breaking the rules of quantum mechanics. In fact, topological insulator is a non-trivial phase in the quantum mechanics, we also call that "Quantum Spin Hall Effect (QSHE)".

The similar case is "Integer Quantum Hall Effect (IQHE)". In 1980, K. v. Klitzing, G. Dorda and M. Pepper [1]. They found the integer conductivity in graphene under the magnetic field. And electrons are moving along the edge. In 1982, Daniel Tsui and Horst Störmer also found the "Fraction Quantum Hall Effect (FQHE)" in the graphene under

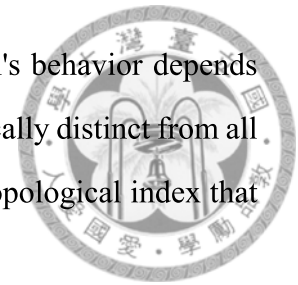

the high magnetic field at the low temperature [2]. Above material's behavior depends only on its topology and not on its specific geometry; it was topologically distinct from all previously known states of matter. And it can be identified by the topological index that is called "TKNN Number" (or Chen Number) [4].

Later, in 2005, C. L. Kane and E. J. Mele found the "Quantum Spin Hall Effect" in the zigzag grphene nano-ribbon with the intrinsic spin-orbit coupling that is the first topological insulator [4]. This effect can be seen as that have a pair of quantum Hall states, and each state are time reversal symmetry by each other. Even though this quantum spin Hall behavior also depends on its topology like the quantum Hall sate. However, the TKNN number do not distinguish this type of topological state since it do not include the considering of time reversal symmetry couple. The new topological index "Z_2 Number" is provided to identify the material is topological material or not, and there are several mathematical formulations of this topological invariant [5] [6] [7] [8] [9] [10] [11].

In this dissertation, two realistic influence in the manufacturing process is considered. First is the geometry influence, we study the transport property in the branch shaped of the 2D topological insulator that is a zigzag honeycomb lattice with intrinsic spin-orbit coupling, we found the property of the transmission and spin polarization is depend on the structure of the device. The second influence is the impurity, in general, the topological insulator is robust for impurities. However, we found the impurity can reduce the transmission in the finite width, because the impurity produce the bound state at specific values of the impurity potential and that provided the passage between two edge states. So the electron go back on the opposite edge when the distance between two edges is close enough. In the last part, we design a device that combine those two influence, the behavior of the transmission is correspond to the Fano resonance [12] and the quantum interference can be described.

The hierarchy of transport models are show in the table figure 1.1. The right model depends on the problem and the accuracy you want, and every method has its pros and cons. In this study, the topological insulator is a material that have a strong spin-orbit coupling. The spin-orbit coupling have a strong relation with quantum mechanics. So, we chose the

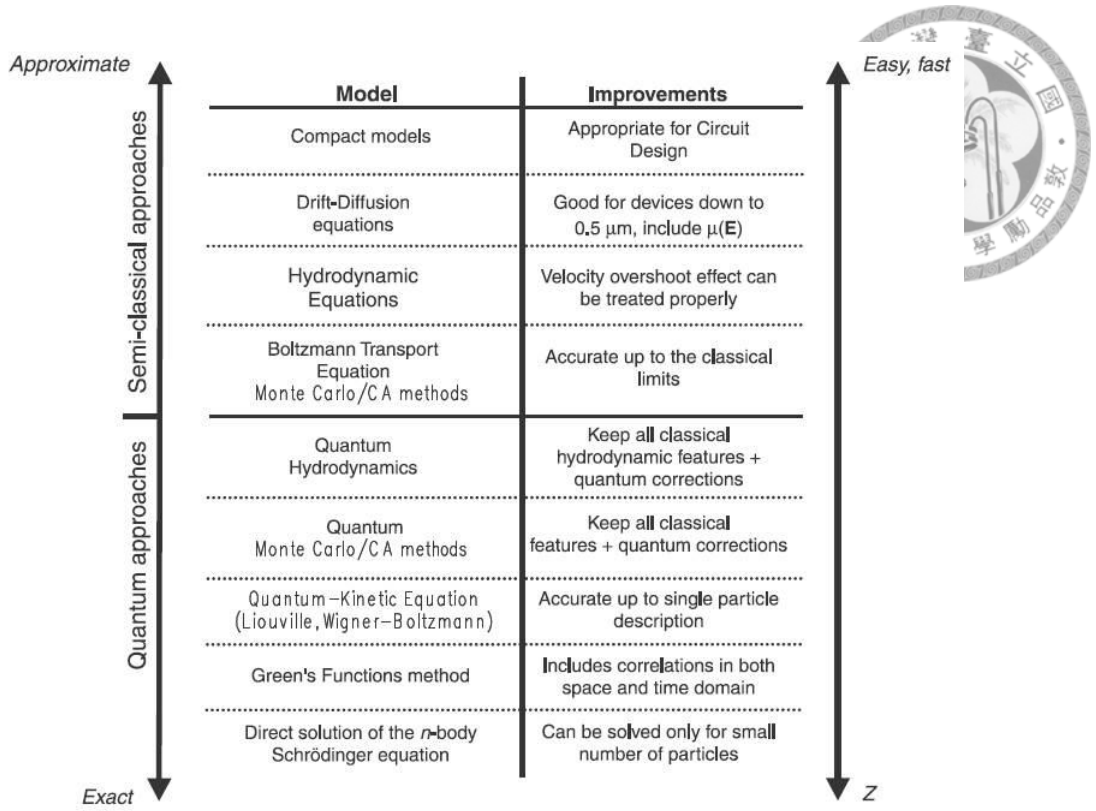

Figure 1.1: (Adapted from [13]) Illustration of the hierarchy of transport models.

Green function method combine with tight-binding method. The common ground of our systems is a device connect with several semi-infinite leads. We used the Landauer step to discuss the transport of those system, and further used Landauer-Keldysh formalism of Non-Equilibrium Green Function to handle the non-equilibrium system (under applied bias).

1.2 Outline of Dissertation

In Chapter 2, the brief introduction of Landauer formalism of tight-binding Green function are presented as well. Next, the introduction of the topological insulator is presented in Chapter 3. We provide the topological view to distinguish the trivial material and topological insulator, and describe the property of the quantum spin Hall effect. Then we introduce the topological index and 2D topological insulator material.

The branch shaped of topological insulator is considered in Chapter 4. As previous mention, the topological insulator is robust in general situation, so we add the impurity in

the finite width HgTe/CdTe quantum well to simulate the realistic system in Chapter 5. In Chapter 6, we design the device of HgTe/CdTe quantum well and found the interesting quantum interference.

In Chapter 4 Chapter 5 and Chapter 6, we used the method of Landauer Formalism from Chapter 2. In the last Chapter, we summarize our study and give an outlook in the field.

Bibliography

[1] K. V. Klitzing, G. Dorda and M. Pepper, Phys. Rev. Lett. **4**5, 494 (1980)

[2] D. C. Tsui, H. L. Stormer, and A. C. Gossard. Phys. Rev. Lett. **4**8 (1559)

[3] Thouless, D. J., M. Kohmoto, M. P. Nightingale, and M. den Nijs, Phys. Rev. Lett. **4**9, 405 (1982)

[4] Kane, C. L., and E. J. Mele. Phys. Rev. Lett. **9**5, 226801 (2005)

[5] Kane, C. L., and E. J. Mele. Phys. Rev. Lett. **9**5, 146802 (2005)

[6] Fu, L., and C. L. Kane. Phys. Rev. B **7**4, 195312 (2006)

[7] Fu, L., and C. L. Kane. Phys. Rev. B **7**6, 045302 (2007)

[8] Fukui, T., and Y. Hatsugai. J. Phys. Soc. Jpn. **7**6, 053702 (2007)

[9] Moore, J. E., and L. Balents. Phys. Rev. B **7**5, 121306 (2007)

[10] Fukui, T., T. Fujiwara, and Y. Hatsugai. J. Phys. Soc. Jpn. **7**7, 123705 (2008)

[11] Qi, X. L., T. L. Hughes, and S. C. Zhang. Phys. Rev. B **7**8, 195424 (2008)

[12] Andrey E. Miroshnichenko, Sergej Flach, and Yuri S. Kivshar. Rev. Mod. Phys. **8**2, 2257

[13] D. Vasileska and S. M. Goodnick. l, Computational Electronics. Morgan and Claypool Publishers, 2006.

Chapter 2

Green Function in Quantum System

2.1 Tight-Binding Model building the Hamiltonian

To building the model for the quantum system. Building a Hamiltonian matrix is an important step at first. In quantum mechanics, Hamiltonian is the operator corresponding to the total energy of the system, and it can be expanded by any basis. In the tight-binding model, we used atomic orbital to expand the Hamiltonian.

$$\hat{H}_{TB} = \sum_{j} \varepsilon_j c_j^{\dagger} c_j + \sum_{i \neq j} t_{ij} c_i^{\dagger} c_j \tag{2.1}$$

where ε_j is the on site energy in the position j,and t_{ij} is the hopping energy between the position i and j. For the example, we consider a six atoms system

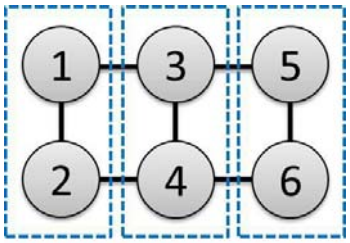

Figure 2.1: An example for the six atoms system.

The Hamiltonian is shown :

$$\hat{H}_{TB}^{(6\times6)} = \begin{bmatrix} \varepsilon_{11} & t_{12} & t_{13} & 0 & 0 & 0 \\ t_{21} & \varepsilon_{22} & 0 & t_{24} & 0 & 0 \\ t_{31} & 0 & \varepsilon_{33} & t_{34} & t_{35} & 0 \\ 0 & t_{42} & t_{43} & \varepsilon_{44} & 0 & t_{46} \\ 0 & 0 & t_{53} & 0 & \varepsilon_{55} & t_{56} \\ 0 & 0 & 0 & t_{64} & t_{65} & \varepsilon_{66} \end{bmatrix} = \begin{bmatrix} \hat{H}_{12}^{(2\times2)} & \tau_{12,34} & 0 \\ \tau_{34,12} & \hat{H}_{34}^{(2\times2)} & \tau_{34,56} \\ 0 & \tau_{56,34} & \hat{H}_{56}^{(2\times2)} \end{bmatrix} \tag{2.2}$$

And diagonalize the Hamiltonian, we can get he energy level E_n, where energy levels $n = 1, 2, 3, 4, 5, 6$.

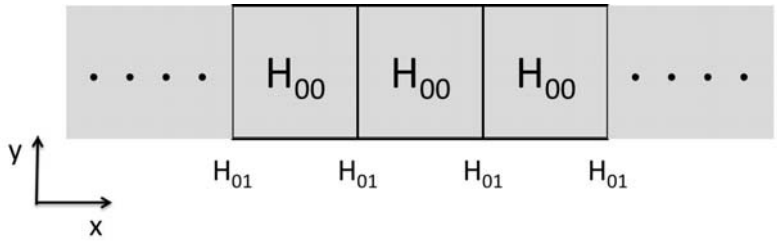

Figure 2.2: An example for the periodical geometry.

To consider the periodical infinite geometry along one direction figure 2.2.The Hamiltonian is expanded by the local atomically basis as

$$\hat{H}_{TB} = \begin{pmatrix} \ddots & \hat{H}_{01} & 0 & 0 \\ \hat{H}_{01}^{\dagger} & \hat{H}_{00} & \hat{H}_{01} & 0 \\ 0 & \hat{H}_{01} & \hat{H}_{00} & \hat{H}_{01} \\ 0 & 0 & \hat{H}_{01} & \ddots \end{pmatrix} \tag{2.3}$$

This is an infinite dimensional matrix, so we should change the basis by *Bloch states*

$$\psi_B\left(\vec{k}\right) = e^{i\vec{k}\cdot\vec{r}} u\left(\vec{r}\right) \tag{2.4}$$

where k is the parameter called the *crystal momentum*.The Hamiltonian is expanded by

the Bloch state basis

$$\hat{H}_k = \hat{H}_{00} + e^{ika}\hat{H}_{01} + e^{-ika}\hat{H}_{01}^{\dagger} \tag{2.5}$$

Energy spectral is plotted

$$\hat{H}_k \Psi_{k,n} = E_n(k)\,\Psi_{k,n} \tag{2.6}$$

The equation is periodic in the k-space of *Brillouin Zone(B.Z.)*, and that is called the *band strucure*.

2.2 Green Function and Local Density of State

In mathematics, Green Function is an impulse response can be used to solve an inhomogeneous differential equation with boundary conditions. We set $\hat{L}$ is an arbitrary linear differential operator as a function of $\phi(x)$

$$\hat{L}\phi(x) = f(x) \tag{2.7}$$

Then, there is a response Green function for the operator $\hat{L}$

$$\hat{L}(x)\,G(x,x') = \delta(x-x') \tag{2.8}$$

With solving this equation, we can easily get the function $\phi(x)$

$$\phi(x) = \int f(x')G(x,x')\,dx' \tag{2.9}$$

In Quantum Mechanics, it also play an important role. First, we write down the Schrödinger equation

$$\{H(\vec{r}) - E_n\}\,\psi_n = 0 \tag{2.10}$$

The wave function

$$\sum_n \psi_n^*(\vec{r})\,\psi_n(\vec{r\prime}) = \delta(\vec{r}-\vec{r\prime}) \tag{2.11}$$

define the Green function

$$\{E_n - H(\vec{r})\} G(\vec{r}, \vec{r}\prime; E) = \delta(\vec{r} - \vec{r}\prime) \tag{2.12}$$

Those wave function ψ_n and operator(H and $G(E)$) are expanded by the real space position basis set $|\vec{r}\rangle$.

$$\psi_n(\vec{r}) = \langle \vec{r} | \psi_n \rangle \tag{2.13a}$$

$$\langle \vec{r} | H | \vec{r}\prime \rangle = H(\vec{r}) \delta(\vec{r} - \vec{r}\prime) \tag{2.13b}$$

$$\langle \vec{r} | G(E) | \vec{r}\prime \rangle = G(\vec{r}, \vec{r}\prime; E) \tag{2.13c}$$

We replace E+iη or E-iη to E, (η is a postive number limite to zero), get retarded G^r and advance G^a green function

$$G^r(E) = G(E + i\eta) \tag{2.14a}$$

$$G^a(E) = G(E - i\eta) \tag{2.14b}$$

The retarded and advance Green function have a relation

$$\hat{G}^a(E) = \hat{G}^{r\dagger}(E) \tag{2.15}$$

Then, we redefine the Green function

$$\{E_n + i\eta - H(\vec{r})\} G^r(\vec{r}, \vec{r}\prime; E) = \delta(\vec{r} - \vec{r}\prime) \tag{2.16}$$

Follow the equation 2.13c, the equation acn be rewritten to

$$\langle \vec{r} | \{E_n + i\eta - H\} G^r(E) | \vec{r}\prime \rangle = \delta(\vec{r} - \vec{r}\prime) \tag{2.17}$$

so

$$G^r(E) = \frac{1}{E + i\eta - H} = \sum_n \frac{|\psi_n\rangle \langle \psi_n|}{E + i\eta - E_n} \tag{2.18}$$

The equation separate the real part and imaginary part.

$$\lim_{y\to 0^+}\frac{1}{x\pm iy}=\frac{P}{x}\mp i\pi\delta\left(x\right) \tag{2.19}$$

use equation 2.19, the imaginary part of the retarded green function can been shown

$$Im\left\{G^r\left(\vec{r},\vec{r}\prime;E\right)\right\}=-i\pi\sum_n\delta\left(E-E_n\right)\psi_n^*\left(\vec{r}\right)\psi_n\left(\vec{r}\right) \tag{2.20}$$

The local density of state

$$\rho\left(\vec{r};E\right)=\sum_n\delta\left(E-E_n\right)\psi_n^*\left(\vec{r}\right)\psi_n\left(\vec{r}\right) \tag{2.21}$$

The local density of state (equation 2.21) correspond to the imaginary part of retarded green function (equation 2.22)

$$\rho\left(\vec{r};E\right)=\frac{i}{\pi}Im\left\{G^r\left(\vec{r},\vec{r};E\right)\right\} \tag{2.22}$$

In the tight-binding model, the retarded green function is a matrix

$$\hat{G}\left(E\right)=\left[\left(E+i\eta\right)\hat{I}-\hat{H}\right]^{-1} \tag{2.23}$$

The equilibrium local density of state for the tight binding model is

$$\left\langle N_{m;\sigma;l}\left(E\right)\right\rangle=\frac{i}{\pi}Im\left\{G^r_{mm;\sigma\sigma;ll}\left(E\right)\right\} \tag{2.24}$$

where m is the site for the electron, σ is the spin and l is the electron orbital.

2.3 Landauer Step

In this section, we use the technique to reduce the matrix dimensions of the green function. If a sample connect other samples, the dimension is depend on this sample that we want two know.

2.3.1 Effective Hamiltonian and Self Energy

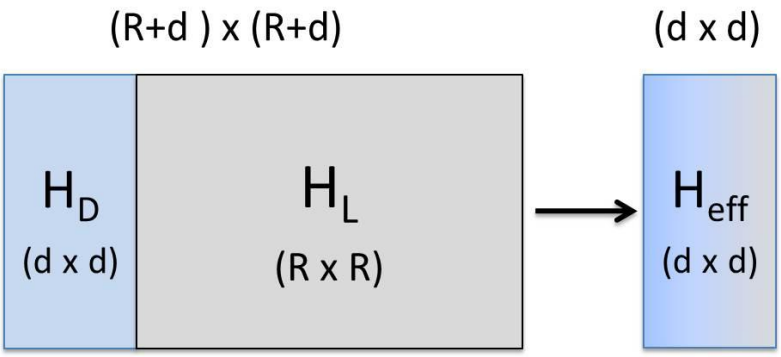

Figure 2.3: An example for two systems coupling together.

In this subsection, two samples are connected to each other figure 2.3. The Hamiltonian for the whole system is

$$\hat{H} = \begin{bmatrix} \hat{H}_D & \hat{H}_{DL} \\ \hat{H}_{DL}^{\dagger} & \hat{H}_L \end{bmatrix} \tag{2.25}$$

The equation

$$\begin{bmatrix} \hat{H}_D & \hat{H}_{DL} \\ \hat{H}_{DL}^{\dagger} & \hat{H}_L \end{bmatrix} \begin{bmatrix} \varphi_D \\ \varphi_L \end{bmatrix} = E_\lambda \begin{bmatrix} \varphi_D \\ \varphi_L \end{bmatrix} \tag{2.26}$$

so, we have

$$\hat{H}_D\varphi_D + \hat{H}_{DL}\varphi_L = E_\lambda\varphi_D \tag{2.27a}$$

$$\hat{H}_{DL}^{\dagger}\varphi_D + \hat{H}_L\varphi_L = E_\lambda\varphi_L \tag{2.27b}$$

$$\varphi_L = \left(E_\lambda - \hat{H}_L\right)^{-1}\hat{H}_{DL}^{\dagger}\varphi_D = \hat{G}_L\left(E_\lambda\right)\hat{H}_{DL}^{\dagger}\varphi_D \tag{2.27c}$$

$$E_\lambda\varphi = \left[\hat{H}_D + \hat{H}_{DL}\hat{G}_L\left(E_\lambda\right)\hat{H}_{DL}^{\dagger}\right]\varphi_D \tag{2.28}$$

So, we define the effective Hamiltonian:

$$\hat{H}_{eff}\left(E_\lambda\right) \equiv \hat{H}_D + \hat{H}_{DL}\hat{G}_L\left(E_\lambda\right)\hat{H}_{DL}^\dagger \tag{2.29}$$

The Green function $\hat{G}_L$ can be called "Surface Green Function" . Then we define the self energy matrix,

$$\hat{\Sigma}\left(E\right) \equiv \hat{H}_{DL}\hat{G}_L\left(E\right)\hat{H}_{DL}^\dagger \tag{2.30}$$

And rewrite the Hamiltonian by the other formalism,

$$\hat{H}_{eff}\left(E\right) = \hat{H} + \hat{\Sigma}\left(E\right) \tag{2.31}$$

Follow the equation 2.23, the retarded Green function for the system 1 (figure 2.3) is

$$\hat{G}^r\left(E\right) = \left[\left(E + i\eta\right)\hat{I} - \hat{H}_D - \hat{\Sigma}\left(E\right)\right]^{-1} \tag{2.32}$$

2.3.2 Surface Green function for Semi-Infinite System

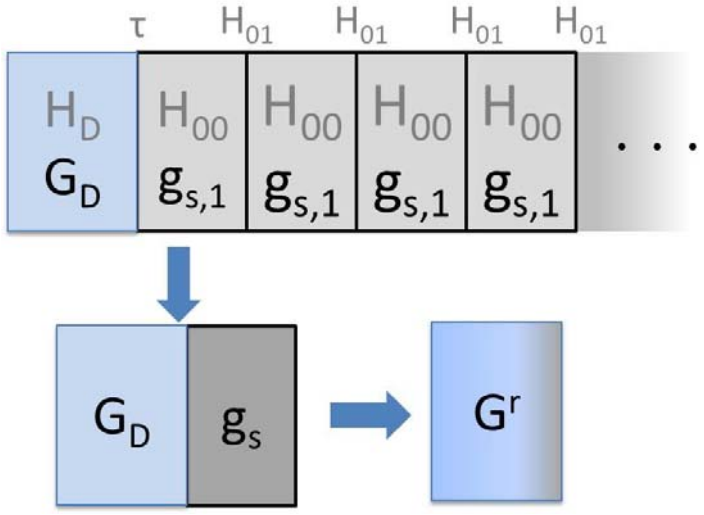

Figure 2.4: The geometry for a device connect a semi-infinite lead.

In this subsection, we discuss about a device connect the semi-infinit lead.We buliding the Hamiltonian for the whole system is follow the equation 2.25. In this geometry, the

Hamiltonian for the lead is an infinite matrix as

$$\hat{H}_L = \begin{bmatrix} \hat{H}_{00} & \hat{H}_{01} & 0 & \cdots \\ \hat{H}_{01}^{\dagger} & \hat{H}_{00} & \hat{H}_{01} & \cdots \\ 0 & \hat{H}_{01}^{\dagger} & \hat{H}_{00} & \cdots \\ \vdots & \vdots & \vdots & \ddots \end{bmatrix} \tag{2.33}$$

In theory, the method in section 2.3.2 should be used unlimited times figure 2.5. The

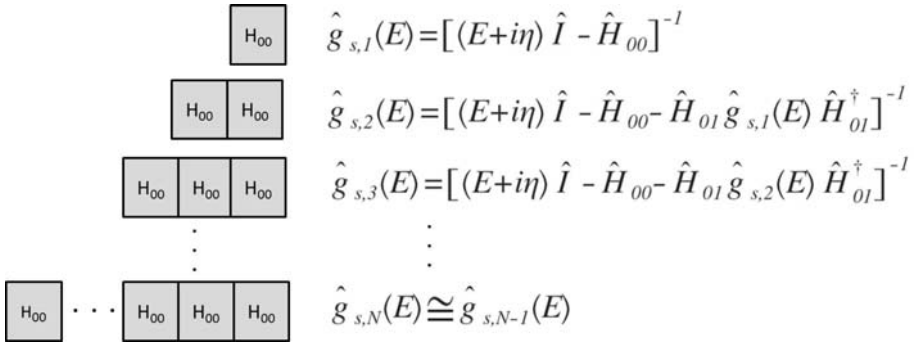

Figure 2.5: The self-consistent process for the semi-infinite periodical geometry.

surface green function for the lead have a recursive equation

$$\hat{g}_s(E) = \left[(E+i\eta)\hat{I} - \hat{H}_{00} - \hat{H}_{01}\hat{g}_s(E)\hat{H}_{01}^{\dagger}\right] \tag{2.34}$$

Follow the equation 2.30, the self energy for the lead is

$$\hat{\Sigma}_p(E) = \hat{\tau}\hat{g}_s(E)\hat{\tau}^{\dagger} \tag{2.35}$$

Where τ is the hopping matrix between the device and one layer of the lead. The retarded green function for the device connected several leads (figure 2.6) is

$$\hat{G}^r(E) = \left[(E+i\eta)\hat{I} - \hat{H}_D - \sum_p \hat{\Sigma}_p(E)\right]^{-1} \tag{2.36}$$

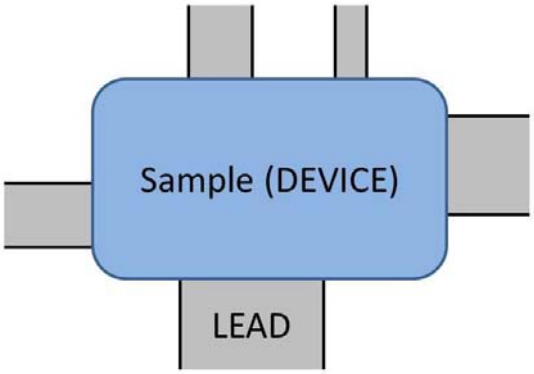

Figure 2.6: The self-consistent process for the semi-infinite periodical geometry.

2.3.3 Landauer-Buttiker Formula

The transmission between two leads is

$$T_{ij} \equiv Tr\left[\hat{\Gamma}_j \hat{G}^r \hat{\Gamma}_i \hat{G}^a\right] \tag{2.37}$$

This equation represent the transmission from lead i to lead j. Where $\hat{\Gamma}_i$ is the broadening matrix

$$\hat{\Gamma}_i \equiv i\left[\hat{\Sigma}_i - \hat{\Sigma}_i^\dagger\right] \tag{2.38}$$

that is related the imaginary part of the self-energy matrix of one lead.

The electron current

$$I_{ij} = \int_{-\infty}^{\infty} \left[Tr\left(\hat{\Gamma}_j \hat{G}^r \hat{\Gamma}_i \hat{G}^a\right)\left(f\left(E - eV_i\right) - f\left(E - eV_j\right)\right)\right] dE \tag{2.39}$$

2.3.4 Landauer-Keldysh Formalism

For the non-equilibrium system, the bias voltage is applied in the lead. The lesser green function should be used

$$\hat{G}^<(E) = \hat{G}^r(E)\,\hat{\Sigma}^<(E)\,\hat{G}^a(E) \tag{2.40}$$

The matrix $\widehat{\Sigma}(E)$ lesser self energy function

$$\widehat{\Sigma}(E) = -\sum_{p}\left[\widehat{\Sigma}_{p}(E - eV_{p}) - \widehat{\Sigma}_{p}^{\dagger}(E - eV_{p})\right] f(E - eV_{p}) \tag{2.41}$$

The equilibrium Fermi-Dirac distribution in each lead is of the form

$$f(E) = \frac{1}{e^{\left(E - E_{f}\right)/k_{b}T} + 1} \tag{2.42}$$

The local particle density

$$\left\langle \hat{N}_{m;\sigma}(E) \right\rangle = \frac{1}{2\pi i}\int_{-\infty}^{\infty} dE G_{mm;\sigma\sigma}^{<}(E) \tag{2.43}$$

The local charge density

$$\left\langle e\hat{N}_{m}(E) \right\rangle = \frac{e}{2\pi i}\int_{-\infty}^{\infty} dE Tr_{s}\left(\hat{G}_{mm}^{<}(E)\right) \tag{2.44}$$

The local spin density

$$\left\langle \hat{s}_{m}(E) \right\rangle = \frac{\hbar}{2}\frac{e}{2\pi i}\int_{-\infty}^{\infty} dE Tr_{s}\left(\hat{\sigma}\hat{G}_{mm}^{<}(E)\right) \tag{2.45}$$

Bibliography

[1] B. K. Nikolić, S. Souma, L. P. Zarrbo, and J. Sinova, Phys. Rev, Lett. **95,** 046601 (2005).

[2] Electronic Transport in Mesoscopic Systems Cambridge University Press, Cambridge, (1995).

[3] Supriyo Datta, Quantum Transport: Atom to Transistor Cambridge University Press, Cambridge (2005).

Chapter 3

Topological Insulator

Recently, topological insulators have attracted intense attention for their novel physics phenomena in materials. A two-dimensional (2D) topological insulator was first predicted in 2005 and several possible materials were proposed. This phenomenon is also called the Quantum Spin Hall Effect and the existence of helical edge (or surface state in three dimension) states is a signature for the quantum transport. In two dimension of topological insulator, the magnitude of the spin Hall conductivity reaches a universal constant $e/4\pi$. In their initial proposal, Kane and Mele proposed that the intrinsic spin-orbit interaction within zigzag graphene nano-ribbon revises the bulk band structure and induces the Dirac cone of the edge state.

The quantum spin Hall phase is a time reversal invariant electronic state with a bulk electronic band gap that supports the transport of charge and spin in gapless edge states. Electrons can be divided into: spin up and down, move to the left and right , four type of states. On the top edge, spin up (down) state electron only move to the right (left); on the below state electron only move to the left (right). The edge states of the quantum spin Hall effect are helical because their spin direction and momentum are locked with each other, and electrons of spin-up and spin-down propagate along the opposite directions on the boundary of the bulk for the time reversal symmetry (figure 3.1).

The QSH state realized here is equivalent to two copies of the quantum Hall effect, in which the two chiral edge states are spin polarized and those form a time-reversed pair to recover the overall time reversal symmetry.

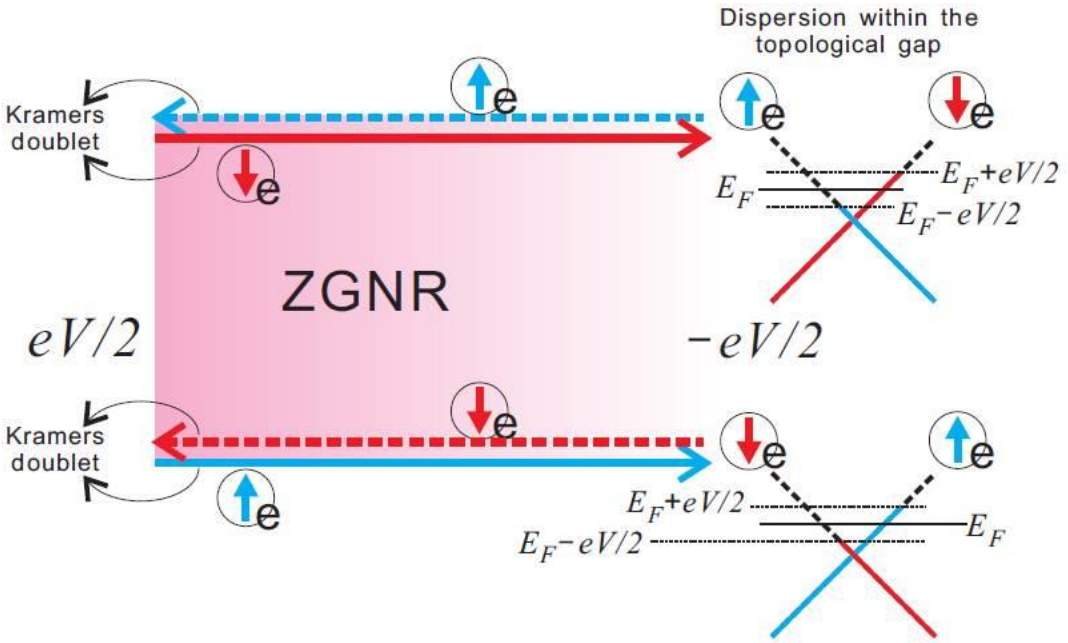

Figure 3.1: Edge currents of TI in a two-terminal setup and (right) electron population. Blue color here is associated with up spin-z and red with down spin. The TI is in contact with two metal leads biased with potential $eV/2$ (for left lead) and $eV/2$ (for right lead). The diagrams to the right shows electron population according to our selected parameters. Black dashed lines are the dispersions with empty populations. Since the slope of the dispersions represents the velocity, on the upper edge, we have a net down spin current moving to the right , while on the lower edge, a net up spin current. The arrows of dashed and solid lines on each TI edge indicate a Kramers doublet.

3.1 The Topology and Band Structure

The band for a semiconductor or insulator is shown in figure 3.2(a), the Fermi level does not intersect either band, blue color is the antisymmetric and valence band; red color is the symmetric and conduction band. This situation is like the bottom picture, symmetric and antisymmetric are different side, not crossover each other.

However, if the spin-orbit coupling is large, it may lead to antisymmetric states have higher energies than symmetric states, it's mean "band inversion". The conduction and valence bands actually crossing over by two linear bands. The one band is spin up another is spin down. As figure 3.2(b) antisymmetric and valence states connect each other. An electron moving along the band in the BZ, it go to another band. This situation is like a Mobius strip, If you go alone one side, you will go to another side. Actually, this topology of the srip only exist one side. We call that is the topological insulator.

Then, the spin-orbit coupling may also cause another situation, the band have two twists, and that have the same topology with figure 3.2(a). An electron moving along the band, it will go to the original point. Even thought, the strip twist two times It still a two side strip like figure 3.2(a) strip, so it is not a topological insulator.

The band structure can also explain why topological insulator is robust. In figure 3.2(b), the surface state with positive momentum is spin down, and negative momentum is spin up. When the electron scatter occur, it's mean positive momentum electron change two negative momentum and the spin will also change. However, if the defect do not have the magnetic property, the spin flip it is not allow, so the electron scattering is not allow. But, in the figure 3.2(c) we can see the down state are still down state through the scattering, so that do not robust with defect.

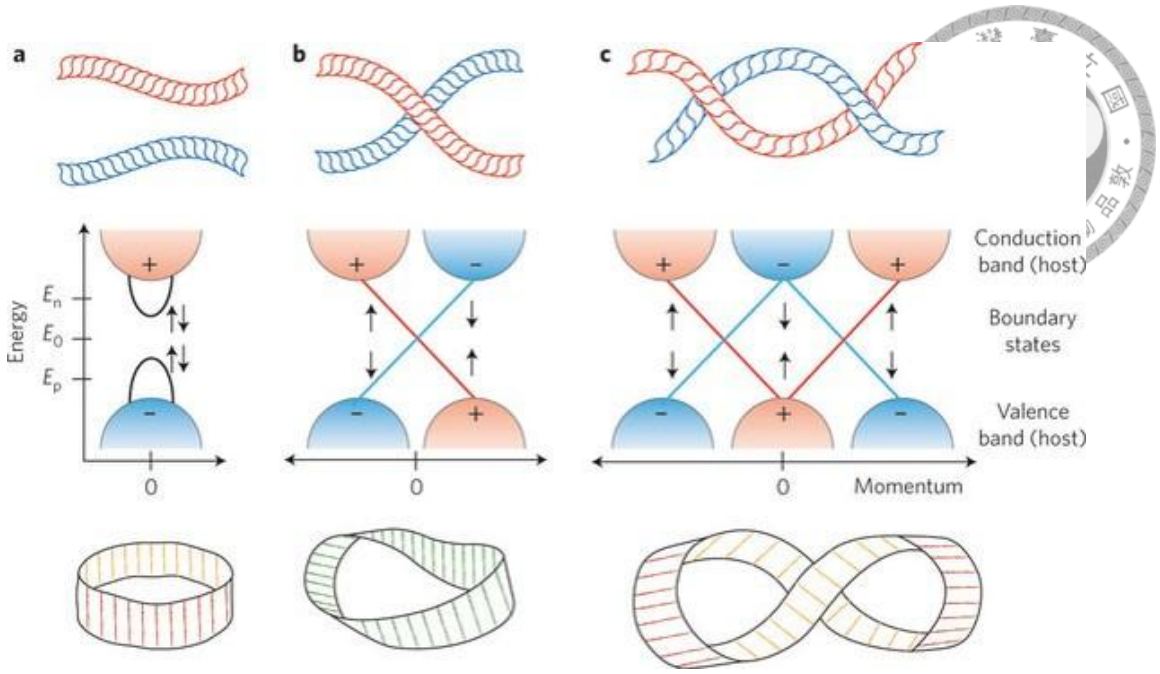

Figure 3.2: (adapted from [1])The topology of the band structure near the fermi energy is depend on the twist between the valence band and conduction band.(a) Zero twist band represent the topological trivial state.(b) One twist band represent the topological non-trivial state (c)Two twist band represent the topological trivial state.

3.2 Topology and Topological Insulator

3.2.1 Berry Connection

Here, we define the Berry connection

$$\vec{A}\left(\vec{R}\right) = \sum_n \vec{a}_n\left(\vec{R}\right) \tag{3.1}$$

and the partial Berry connection by one state

$$\vec{a}_n\left(\vec{R}\right) = -i\left\langle n, \vec{R}\right| \vec{\nabla}_R \left|n, \vec{R}\right\rangle \tag{3.2}$$

The Berry connection corresponds to the gauge field defined on that parameter space, similar to the vector potential for electromagnetic fields in real space. Berry curvature is

$$\vec{F}\left(\vec{R}\right) = \vec{\nabla}_R \times \vec{A}\left(\vec{R}\right) \tag{3.3}$$

The position $\vec{R}$ is moves on a closed loop C from $t = 0$ and returns to the original

position at $t = T$ so that $\vec{R}(0) = \vec{R}(T)$, the Berry phase for the loop C is defined as

$$\gamma_n [C] = -\oint_C d\vec{R} \cdot \vec{a}_n \left(\vec{R}\right) \tag{3.4}$$

Berry phase is the is the geometric phase, and it accumulated phase factor of a quantum-mechanical system after it completes a closed path in the parameter space.

3.2.2 Integer Quantum Hall Effect and TKNN Invariant (Chern Number)

The TKNN Invariant is a topological invariant defined for the integer quantum Hall effect. The Berry connection is written for Bloch states in the BZ of momentum space, the one band partial Berry connection is

$$\vec{a}_n \left(\vec{k}\right) = -i \left\langle u_n \left(\vec{k}\right) \middle| \vec{\nabla}_k \middle| u_n \left(\vec{k}\right) \right\rangle \tag{3.5}$$

and we known that $\vec{A}\left(\vec{k}\right) = \sum_n \vec{a}_n \left(\vec{k}\right)$

Berry curvature is also presented in the momentum space as

$$\vec{F}\left(\vec{k}\right) = \vec{\nabla}_k \times \vec{A}\left(\vec{k}\right) \tag{3.6}$$

The Hall conductivity is

$$\sigma_{xy} = \frac{Ne^2}{h} \tag{3.7}$$

The N is the number of Landau levels below the Fermi energy, and the quantization of σ_{xy} is extremely robust. Using the Kubo formula, we can show that the Hall conductivity directly connect with the first Chern number [4].

$$\upsilon_n = \frac{1}{2\pi} \int_{B.Z.} d^2 k \vec{F}_n \left(\vec{k}\right) \tag{3.8}$$

this index is related to the Berry phase as equation 3.4.

$$\upsilon_n = -\frac{1}{2\pi}\gamma_n \left[\partial BZ\right] \tag{3.9}$$

So, the Hall conductivity is always quantized [5] according to the Berry phase is an integer multiple of 2π after encircling the Brillouin zone boundary (∂BZ).

3.2.3 Z_2 Topological Insulator

In quantum spin Hall state, due to the time reversal symmetry, the Berry curvature is an odd function of k_x and k_y, This property guarantees that the Chern number always is zero from equation **??**. In order to classify topological insulator and normal insulator into different group, the new index should be determine that is Z_2 number [6] [7] [8] [9].

We study a family of one-dimensional Hamiltonians that have a bulk energy gap and a length that is much larger than the exponential attenuation length associated with that gap. The Hamiltonians satisfies the following conditions:

$$H\left(t+T\right) = H\left(t\right) \tag{3.10}$$

$$H\left(-t\right) = \Theta H\left(t\right)\Theta^{-1} \tag{3.11}$$

The charge polarization can be calculated by integrating the Berry connection of the occupied states over the BZ.

$$P_c = \int_{-\pi}^{\pi} \frac{dk}{2\pi} A\left(k\right) \tag{3.12}$$

Consider that $2N$ bands are occupied and forming N Kramers pairs. For each Kramers pair n, at the TR symmetric times $t = 0$ and π the wave functions are related by

$$\Theta\left|u_2^n\left(k\right)\right\rangle = e^{-i\chi_n(k)}\left|u_1^n\left(-k\right)\right\rangle \tag{3.13}$$

$$\Theta\left|u_1^n\left(k\right)\right\rangle = -e^{-i\chi_n(-k)}\left|u_2^n\left(-k\right)\right\rangle \tag{3.14}$$

one may obtain

$$A_1(-k) = A_2(k) - \frac{\partial}{\partial k}\chi(k) \tag{3.15}$$

The ω matrix is definied by the time reversed wave functions

$$\begin{aligned}
\omega_{21,nn}(k) &= \langle u_2^m(-k)|\,\Theta\,|u_1^n(k)\rangle = -\delta_{mn}e^{-i\chi_n(k)}, \\
\omega_{12,nn}(k) &= -\omega_{21,nn}(-k)
\end{aligned} \tag{3.16}$$

and the ω matrix is given by

$$\begin{aligned}
\omega(k) &= \begin{bmatrix}
0 & \omega_{12,11} & 0 & 0 & \cdots \\
\omega_{21,11} & 0 & 0 & 0 & \cdots \\
0 & 0 & 0 & \omega_{12,22} & \cdots \\
0 & 0 & \omega_{21,22} & 0 & \cdots \\
\vdots & \vdots & \vdots & \vdots & \ddots
\end{bmatrix} \\
&= \begin{bmatrix}
0 & e^{-i\chi_1(k)} & 0 & 0 & \cdots \\
-e^{-i\chi_1(-k)} & 0 & 0 & 0 & \cdots \\
0 & 0 & 0 & e^{-i\chi_2(k)} & \cdots \\
0 & 0 & -e^{-i\chi_2(-k)} & 0 & \cdots \\
\vdots & \vdots & \vdots & \vdots & \ddots
\end{bmatrix}
\end{aligned} \tag{3.17}$$

This is a skew matrix, it satisfies the condition $-\omega = \omega^T$ and $\omega_{ij} = -\omega_{ji}$

The contribution from each band may be called partial polarization defined by

$$P_i = \int_{-\pi}^{\pi} \frac{dk}{2\pi} A_i(k) \tag{3.18}$$

the time-reversal polarization is defined by

$$P_{TR} = P_1 - P_2 = 2P_1 - P_c \tag{3.19}$$

To make this invariance explicit for P_1, we treat the portions of the integral for positive

and negative k separately

$$\begin{aligned} P_1 &= \int_{-\pi}^{\pi} \frac{dk}{2\pi} A_1(k) \\ &= \int_0^{\pi} \frac{dk}{2\pi} A_1(k) - \int_0^{\pi} \frac{dk}{2\pi} A_1(-k) \\ &= \int_0^{\pi} \frac{dk}{2\pi} A(k) - \frac{1}{2\pi} \sum_{n=1}^{N} [\chi_n(\pi) - \chi_n(0)] \end{aligned} \tag{3.20}$$

then we know that

$$\omega_{12,11}(\Lambda_i)\,\omega_{12,22}(\Lambda_i)\ldots\omega_{12,NN}(\Lambda_i) = e^{-i\sum_{n=1}^{N}\chi_n(\Lambda_i)} = Pf[\omega(\Lambda_i)] \tag{3.21}$$

follow the equation 3.16, and reduces to

$$P_1 = \int_0^{\pi} \frac{dk}{2\pi} A(k) - \frac{i}{2\pi} \ln \frac{pf[\omega(\pi)]}{pf[\omega(0)]} \tag{3.22}$$

So, the time-reversal polarization become

$$P_{TR} = \int_0^{\pi} \frac{dk}{2\pi} (A(k) - A(-k)) - \frac{i}{\pi} \ln \frac{pf[\omega(\pi)]}{pf[\omega(0)]} \tag{3.23}$$

follow the equation 3.13, the equation become

$$\begin{aligned} P_{TR} &= \int_0^{\pi} i\frac{dk}{2\pi} tr\left[\omega^{\dagger}(k) \frac{\partial}{\partial k}\omega(k)\right] - \frac{i}{2\pi} \ln \frac{pf[\omega(\pi)]}{pf[\omega(0)]} \\ &= \int_0^{\pi} i\frac{dk}{2\pi} \frac{\partial}{\partial k} \ln(det[\omega(k)]) - \frac{i}{2\pi} \ln \frac{pf[\omega(\pi)]}{pf[\omega(0)]} \\ &= \frac{i}{\pi}\frac{1}{2} \ln \frac{det[\omega(\pi)]}{det[\omega(0)]} - \frac{i}{2\pi} \ln \frac{pf[\omega(\pi)]}{pf[\omega(0)]} \end{aligned} \tag{3.24}$$

Since $det[\omega] = Pf[\omega]^2$, the equation reduces to

$$P_{TR} = \frac{1}{i\pi} \sum_{n=1}^{N} \ln \frac{\sqrt{\omega_{12,nn}(0)^2}}{\omega_{12,nn}(0)} \frac{\omega_{12,nn}(\pi)}{\sqrt{\omega_{12,nn}(\pi)^2}} \tag{3.25}$$

and, in general, Pfaffian is defined for an antisymmetric matrix and is related to the

determinant by

$$Pf[\omega]^2 = det\,[\omega] \tag{3.26}$$

So

$$P_{TR} = \frac{1}{i\pi} \ln \frac{\sqrt{det\,[\omega\,(0)]}}{Pf\,[\omega\,(0)]} \frac{Pf\,[\omega\,(\pi)]}{\sqrt{det\,[\omega\,(\pi)]}} \tag{3.27}$$

We now consider the change of P_{TR}

$$\Delta = P_{TR}\,(T/2) - P_{TR}\,(0) \tag{3.28}$$

This is the Z_2 spin pump [6]

We may write this invariant as

$$(-1)^{\Delta} = \prod_{i=1}^{4} \frac{Pf\,[\omega\,(\Lambda_i)]}{\sqrt{det\,(\omega\,(\Lambda_i))}} \tag{3.29}$$

This is the Z_2 topological invariant, for the 2D system, the space (k, t) change to (k_x, k_y). In fact, there are several methods to compute this index. However, the equation 3.29 is a gauge invariant method. So, this is a more reliable method.

3.3 2D Topological Insulator Material

In this section, we show two materials those are 2D topological insulator. The first material is Zigzag Honeycomb Nano-ribbon with spin-orbi coupling, the second material is a semiconductor system that is CdTe/HgTe/CdTe quantum well.

3.3.1 Zigzag Honeycomb Nano-Ribbon

At beginning the 2DTI phase is proposed existing in zigzag honeycomb nano-ribbon. When we consider the intrinsic spin-orbit in the system, a linear band for the edge state is present, which is an important condition of the QSHE [10] [11]. This is the tight-binding

Hamiltonian for the π-electrons interacting with the localized moment.

$$H^{GNR} = -t \sum_{\langle m,m\prime\rangle;\sigma} c^{\dagger}_{m\tilde{\sigma}} c_{m\prime\tilde{\sigma}\prime} + \frac{2i}{\sqrt{3}} t_{SO} \sum_{\langle\langle m,m\prime\rangle\rangle;\sigma,\sigma\prime=\uparrow\downarrow} c^{\dagger}_{m\tilde{\sigma}} (\sigma_z) \left(\vec{d}_{m\prime,m\prime\prime} \times \vec{d}_{m,m\prime}\right) c_{m\prime\tilde{\sigma}\prime} \tag{3.30}$$

First term is the nearst-nighber term. And the second term is the next nearest neighbor term that is from intrinsic spin-orbit coupling that is the major term to cause quantum spin hall effect.

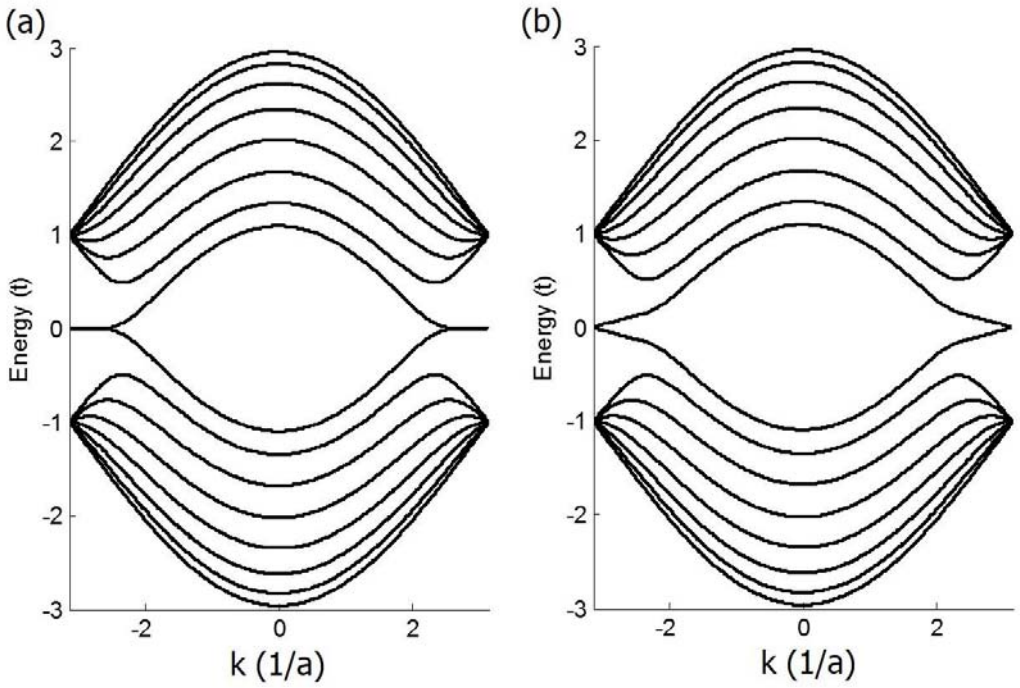

Figure 3.3: The band structure of zigzag honeycomb lattice $N = 8$ (16 atoms in one cell). (a) Without spin-orbit coupling $t_{SO} = 0$ (b) The spin-orbit coupling $(t_{SO} = 0.03\ t)$ produce the linear band near the energy $E = 0$

The band structure show the transition from the normal metal to the topological insulator in the zigzags honeycomb nano-ribbon. In figure 3.3(a), we do not consider the intrinsic spin-orbit in the system, the band structure show that the material is a normal metal with two degenerate flat bands near he fermi energy equal to zero $E = 0$. In figure 3.3(b), where we add the intrinisc spin-orbit coupling with $t_{SO} = 0.03\ t$, it can be found the band structure is open, and those two flat band change to the linear band near $E = 0$. The electron in the linear band is a topological state.

3.3.2 HgTe/CdTe Quantum Well

The HgTe quantum well is a reported topological insulator with both edge energy dispersion and transport phenomenon. The HgTe material transit from normal insulator to topological insulator by changing the thickness of the well region figure 3.4.

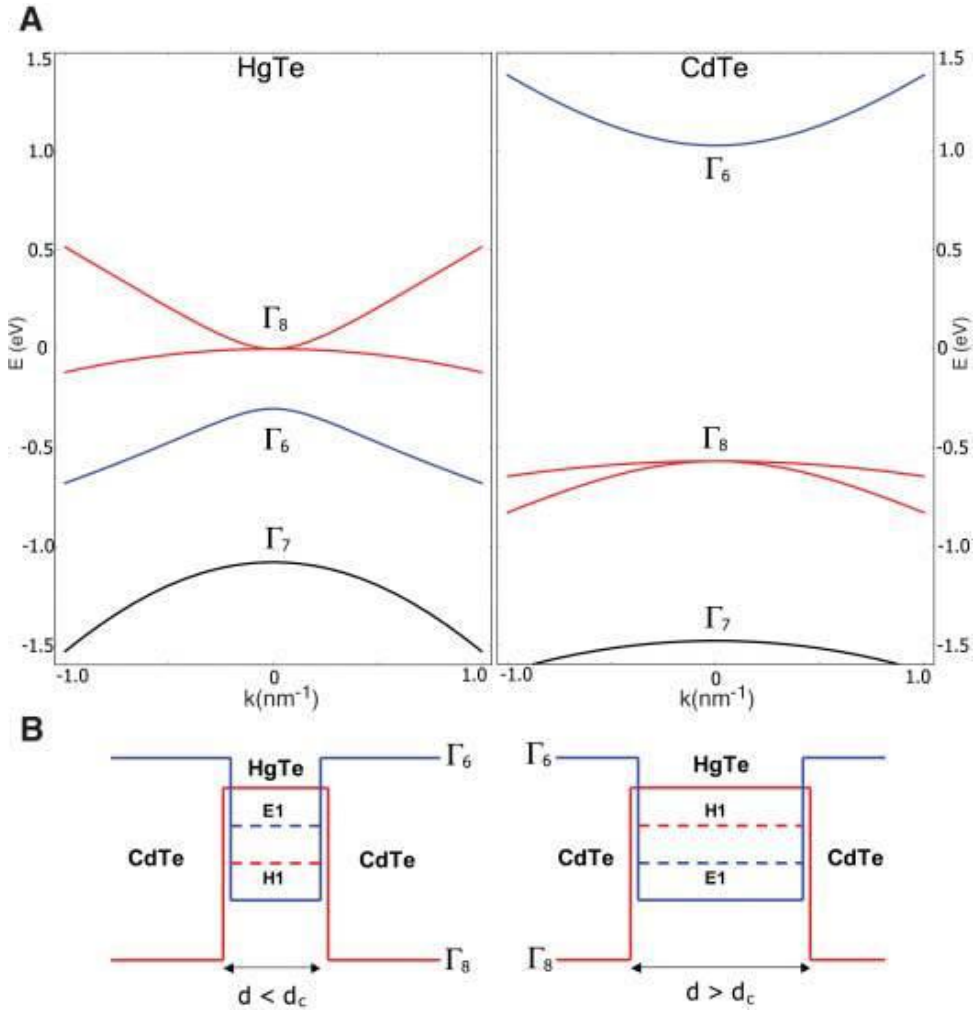

Figure 3.4: (Adapted from [3]) (a) The band structure of HgTe and CdTe near the Γ point. (b) When $d < d_c$) The CdTe-HgTe-CdTe quantum well in the normal condition $E_1 > H_1$ with $d > d_c$ (left) and in the inverted condition $H_1 > E_1$ with $d > d_c$ (right). In this figures, Γ_8/H_1 symmetry is indicated in red and G_6/E_1 symmetry is indicated in blue.

The effective Hamiltonian for the HgTe quantum well can be expressed in a block-diagonal form [3]

$$\mathbf{H} = \begin{bmatrix} \mathbf{h} & 0 \\ 0 & \mathbf{h}^* \end{bmatrix}. \tag{3.31}$$

In this Hamiltonian, the upper 2×2 block is expanded by two pseudo-spin up states

$|s,\uparrow\rangle$ and $|p_x + ip_y,\uparrow\rangle$, and the lower block is for pseudo-spin down states $|s,\downarrow\rangle$ and $|-p_x + ip_y,\downarrow\rangle$. In the tight-binding approximation, the Hamiltonian can be expressed as

$$\begin{aligned}
\mathbf{H}_{TB} = &\sum_{\mathbf{i}} \varphi_{\mathbf{i}}^{\dagger} \begin{bmatrix} E_{is} & 0 & 0 & 0 \\ 0 & E_{ip} & 0 & 0 \\ 0 & 0 & E_{is} & 0 \\ 0 & 0 & 0 & E_{ip} \end{bmatrix} \varphi_{\mathbf{i}} \\
&+ \sum_{\mathbf{i}} \varphi_{\mathbf{i}}^{\dagger} \begin{bmatrix} V_{ss} & V_{sp} & 0 & 0 \\ -V_{sp}^{*} & V_{pp} & 0 & 0 \\ 0 & 0 & V_{ss} & V_{sp}^{*} \\ 0 & 0 & -V_{sp} & V_{pp} \end{bmatrix} \varphi_{\mathbf{i}+\delta\mathbf{x}} + H.c. \\
&+ \sum_{\mathbf{i}} \varphi_{\mathbf{i}}^{\dagger} \begin{bmatrix} V_{ss} & iV_{sp} & 0 & 0 \\ iV_{sp}^{*} & V_{pp} & 0 & 0 \\ 0 & 0 & V_{ss} & -iV_{sp}^{*} \\ 0 & 0 & -iV_{sp} & V_{pp} \end{bmatrix} \varphi_{\mathbf{i}+\delta\mathbf{y}} + H.c. \qquad (3.32)
\end{aligned}$$

by introducing the spinor $\varphi = \left[c_{s,\mathbf{i}}^{\uparrow}, c_{p,\mathbf{i}}^{\uparrow}, c_{s,\mathbf{i}}^{\downarrow}, c_{p,\mathbf{i}}^{\downarrow}\right]^{T}$. Here the index $\mathbf{i}$ represents the lattice site in the real space, then δx and δy are unit vectors along the x and y directions, respectively. Those parameters for on-site energy are: $E_s = C + M - 4(B+D)/a^2$, and $E_p = C - M - 4(D-B)/a^2$. For the hopping energy term $Vsp = -iA/2a$, $V_{ss} = (B+D) = a^2$, $V_{pp} = (D-B)/a^2$. Here a is the lattice constant chosen as $5\ nm$ and the other parameters are $A = 364.5\ meV \cdot nm$, $B = -686\ meV \cdot nm^2$, $C = 0$, $D = -52\ meV \cdot nm^2$. The value of M is a function of thickness of the quantum wells which decides whether the material is topologically trivial or non-trivial. Here we choose $M = -10\ meV$ for a topological insulator. These parameters are controllable in experiment [2] [3].

Bibliography

[1] Hari C. Manoharan. Nature Nanotechnology **5**, 477–479 (2010)

[2] M. Konig, S. Wiedmann, C. Brune, A. Roth, H. Buhmann, L. W. Molenkamp, X. L. Qi, and S. C. Zhang, Science **318**, 766 (2007).

[3] B. A. Bernevig, T. L. Hughes, and S. C. Zhang, Science, **314**, 5806 (2006).

[4] D. J. Thouless, M. Kohmoto, M. P. Nightingale, and M. den Nijs. Phys. Rev. Lett, **49(6)** 405–408 (1982)

[5] D. Xiao, M.-C. Chang, and Q. Niu, Rev. Mod. Phys., **82(3)** 1959–2007 (2010).

[6] L. Fu and C. L. Kane, Phys. Rev. B **74**, 19531 (2006).

[7] L. Fu and C. L. Kane. Phys. Rev. B, **7**6(4):045302 (2007)

[8] L. Fu, C. L. Kane, and E. J. Mele. Phys. Rev. Lett., **9**8(10):106803 (2007).

[9] Yoichi ANDO, Journal of the Physical Society of Japan **82** 102001 (2013).

[10] C. L. Kane and E. J. Mele. Phys. Rev. Lett. **95(22)**:226801, (2005).

[11] C. L. Kane and E. J. Mele. Phys. Rev. Lett. **95(14)**:146802, (2005).

Chapter 4

Spin Transport Calculation for Branch-Shaped 2D Topological Insulator

In this section, we use the Landauer method to calculate the current and polarization on two types of branching topological insulator (fork-shaped and H-shaped). Our results indicate that the branch-shape topological insulator device will enhance the spin polarizing current.

4.1 Introduction

The topological insuator has a novel physical property called the quantum spin Hall effect (QSHE)(Chapter 3). The small bias voltage would split the spin and allow electrons to be distributed to the edges. This phenomenon inspired us to investigate two types of branch-shaped devices of 2D TI The first type is the "fork-shaped TI", which connects with a two branch TI channel, and the second type is the "H-shaped TI", which connects the branch channel on the left and right sides. We can find the current polarization current on both systems by the equation

$$P_{\uparrow(\downarrow)} \equiv \frac{I_{\uparrow(\downarrow)} - I_{\downarrow(\uparrow)}}{I_{\uparrow} + I_{\downarrow}} \tag{4.1}$$

Then we found different transport properties exist for H-shaped TI.

This study we consider the zigzag honeycomb nano-ribbon (ZNR) and HgTe/CdTe quanum well both materials, and we used the non-equilibrium Green function (NEGF) of the Landauer formula (Chapter 2) to compute the numerical results for the system.

4.2 The Investigated Systems in ZNR

ZNR can be a 2D topological insulator, if we consider the spin-orbit coupling on the Hamiltonian, a linear band for the edge state is present, which is an important condition of the QSHE in Chapter 3. We considered two types of geometry, and supposed the electron had a coherent transport at zero temperature, and we ignored the disorder and coulomb repulsion in the sample. The parameters used here are $t = 2.7\ eV$, and $t_{SO} = 0.03\ t$ which were frequently adapted for the graphene system [5]- [7]. (problems related to the multi-terminal graphene device have previously been discussed). [1]– [4]

4.2.1 Fork-Shaped ZNR

The device consists of $N = 10$ ZNR connected by two $N = 4$ ZNRs, as shown in figure 4.1(a). A semi-infinite hole defect is present on the left side. Therefore, we suppose this structure and the complete ZNR to have a similar bulk and edge state energy range $|E| > 0.42\ t$ and $|E| < 0.42\ t$.

Equilibrium case

In figure 4.2, we compare the transmission for the fork-shaped ZNR and the complete ZNR. The semi-infinite defect decreases the transmission at the bulk states, but did not affect edge states transmission. We plotted the local transmission for LEAD2 to LEAD1 and showed that, at the edge state, only the spin down state allowed on LEAD1.

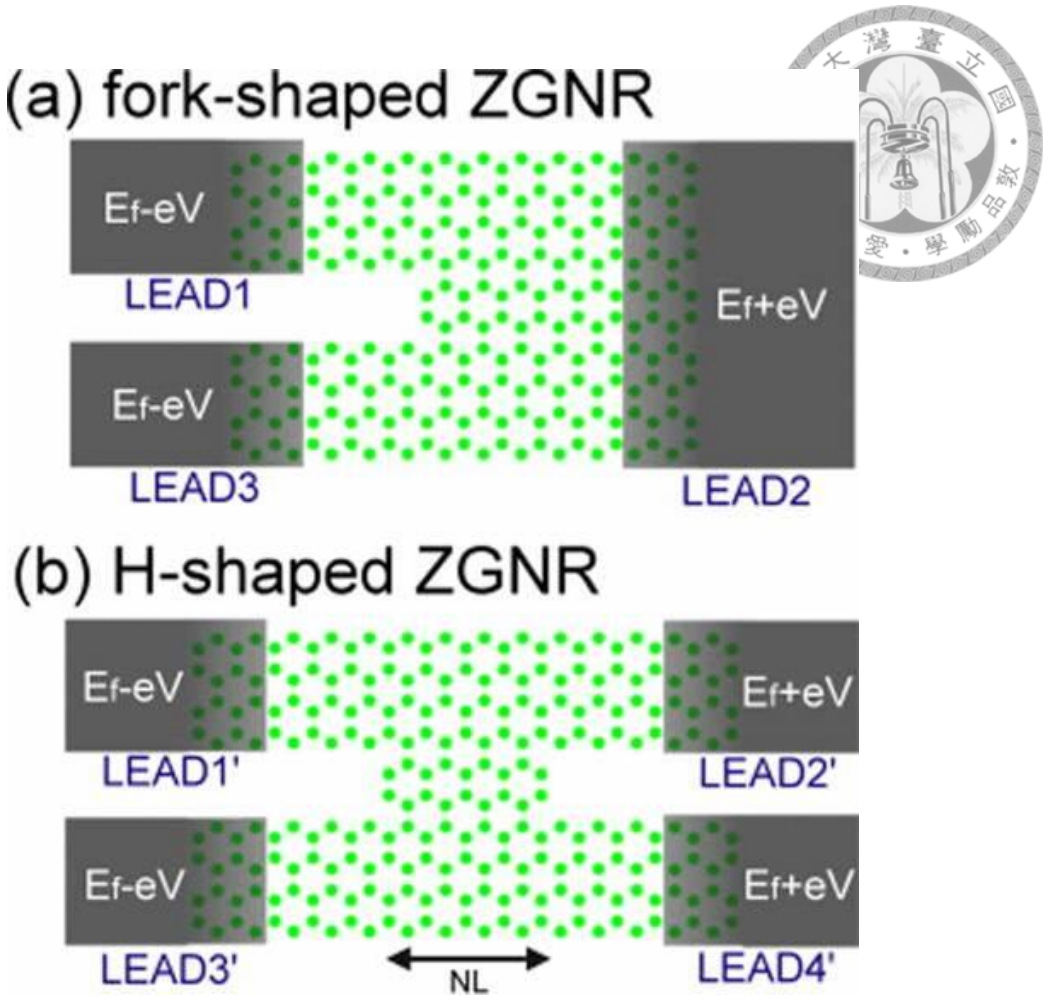

Figure 4.1: Schematic of two branch-shaped ZNR devices (a) $N = 10$ ZNR connected with two $N = 4$ ZNRs channels.(b) $N = 10$ ZNR connected with four $N = 4$ ZNR channels.

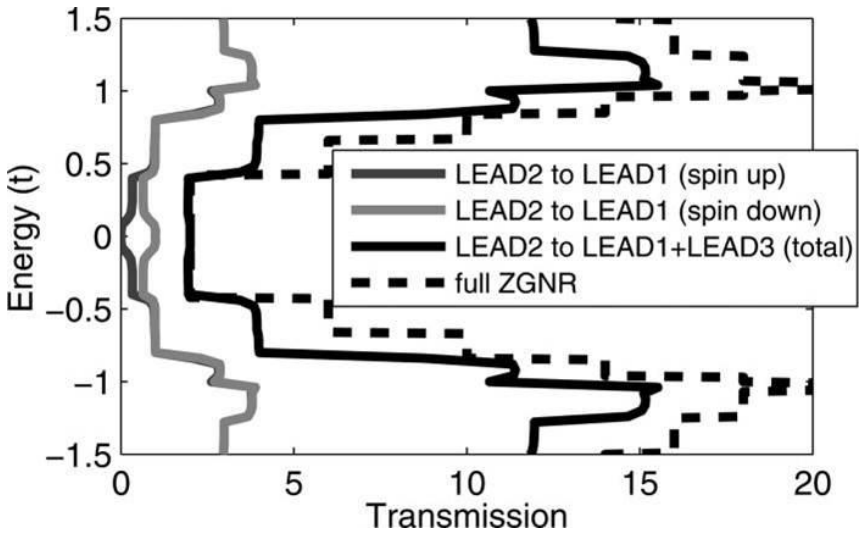

Figure 4.2: Transmission for equilibrium case. The fork-shaped ZNR (real block line), the transmission on LEAD1 (up and down for dark grey and light grey line), and the $N = 10$ ZNR (dashed line).

Non-Equilibrium case

We then set the Fermi energy at 10^{-6} t to understand the behavior at the edge state; the applied small bias was set to $+eV$, $-eV$, and $+eV(eV = 0.0002\ t)$ on the LEADs 1, 2, and 3. The result of spin current polarization on LEAD1 was 0.90. In figure 4.3, the spin density accumulation demonstrates that this defect would not scatter the edge state electron. Conduction electrons occupied the edges such as in a complete ZNR. Conversely, edge electrons did not move to the inner edges.

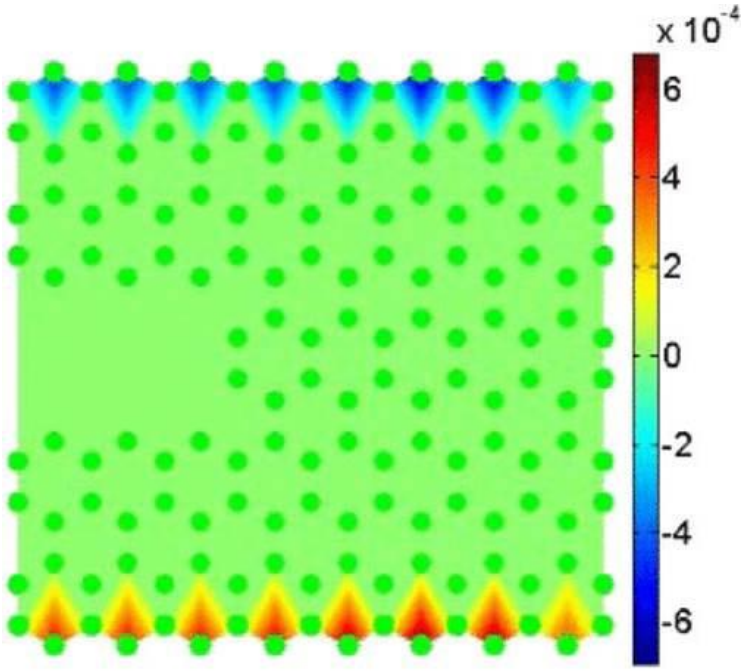

Figure 4.3: The spin density for the fork-shaped ZNR. The Fermi energy at 10^{-6} t and the bias voltage $eV = +\,(-)\,0.0002\ t$ on the right(left) side leads.

4.2.2 H-shaped ZNR

The device consisted of $N = 10$ ZNR connected with four $N = 4$ ZNR. Several types of this geometry were present for N_L as shown in figure 4.1(b). Two arrangements were in this geometry: first, two semi-infinite holes on the left and right sides at $N = 10$ ZNR; and second, two $N = 4$ ZNR were connected to each. This study used the second arrangement to determine the bulk and edge state energy range $|E| > 0.8\ t$ and $|E| < 0.8\ t$, because the source terminals were $N = 4$ ZNR.

Equilibrium case

Consider the $E = 0$ situation: In figure 4.4(a), the transmission (LEAD2'+4' to LEAD1'+3') for the H-shaped ($N_L = 5$) ZNR was larger than 2, and the local transmission (LEAD2'+4' to LEAD1') for spin up and down were similar. In figure 4.4(b), the transmission for the H-shaped ($N_L = 21$) ZNR was close to 2, and the local transmission (LEAD2' +4' to LEAD1') for spin was close to zero. It appears that the transport property depends on the length for the rendezvous area.

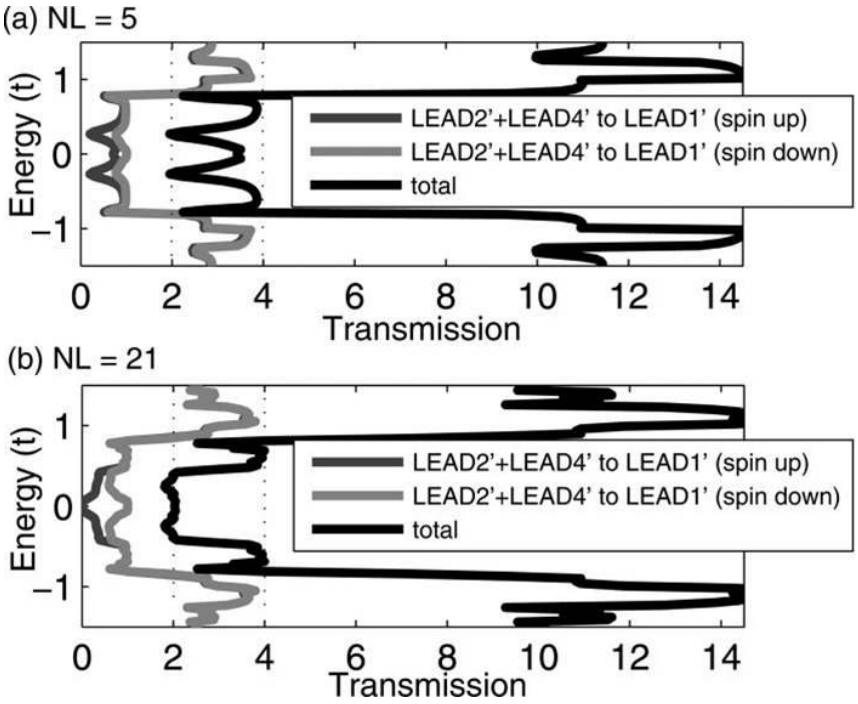

Figure 4.4: Transmission for the equilibrium case. The H-shaped ZNR (real block line) and transmission on LEAD1' (up and down for dark grey and light grey line)(a) $N_L = 5$ and (b) $N_L = 21$.

Non-Equilibrium case

We then set the Fermi energy at $10^{-6}t$ to understand the behavior near the Dirac cone. The applied small bias was set at $+eV$ on LEAD2' and 4', then set $-eV$ on LEAD1' and 3'($eV = 0.0002\ t$).

In figure 4.5, the spin down current on LEAD1' change with N_L. For $N_L < 19$, the spin down current and current polarization was attenuating in an oscillatory manner with increasing N_L; and for $N_L > 19$, the spin down current was close to 0, and current

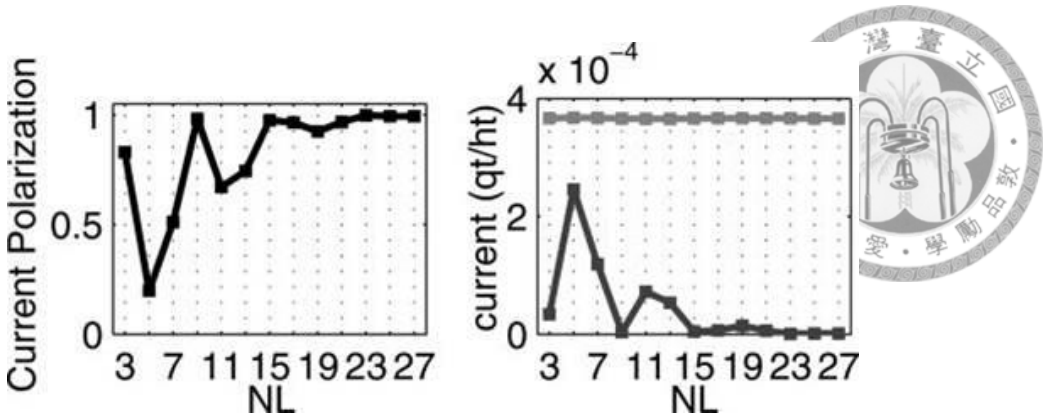

Figure 4.5: The spin current polarization (left) and current for spin up (dark grey) and down (light grey) (right) on LEAD1' with N_L.

polarization was close to 1. A number of local spin density areas were observed in the rendezvous region [see figure 4.6(a)]. However, for $N_L = 21$, they did not form [see figure 4.6(b)].

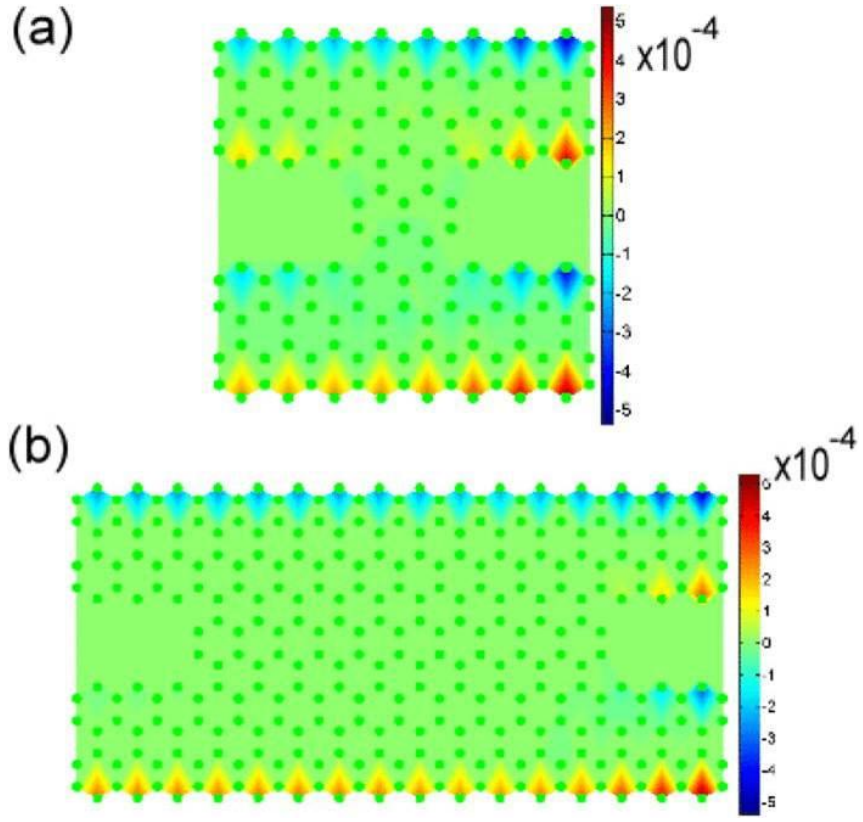

Figure 4.6: The spin density for the H-shaped ZNR. The Fermi energy at 10^{-6} t and the bias voltage $eV = +(-)\,0.0002$ t on the right (left) side leads. (a) $N_L = 5$ and (b) $N_L = 21$.

Therefore, the H-shaped ZNR was divided into two types of structures at $E = 0$: 1. For the smaller rendezvous region ($N_L < 19$): The outer edge electron still contained the

complete density after passage through the rendezvous region. A number of inner edge electrons passed through this area but others returned. The ratio was sensitive to N_L. 2. For the larger rendezvous region ($N_L > 19$): The outer edge still contained complete spin density after the central area, but the inner edge electrons scattered backwards. Actually, in this system only the outer edge states pass to the other lead. This result is similar to transport in fork-shaped samples, but different mechanisms of backward scattering were present here.

4.3 The Investigated Systems in HgTe/CdTe Quantum Well

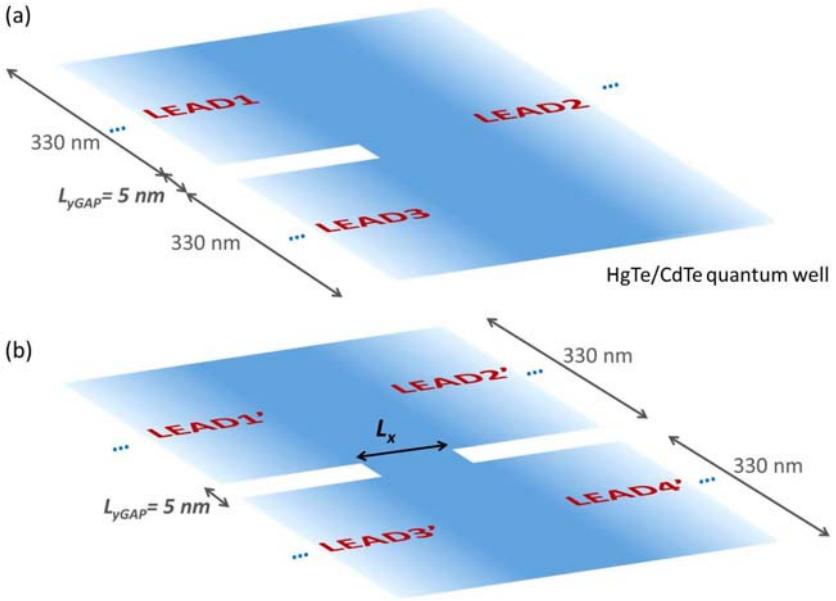

Figure 4.7: Schematic of two branch-shaped HgTe quantum wells. (a) Fork-shaped structure with three leads. (b) H-shaped structure with four leads.

The CdTe/HgTe/CdTe system has a strong intrinsic spin-orbit interaction and it is a reported 2D topological insulator with both edge energy dispersion and transport phenomenon [8].

4.3.1 Fork-shaped HgTe/CdTe Quantum Well

The device consists of $width = 665\ nm$ HgTe QW connected by two $width$ HgTe QWs, as shown in figure 4.7(a). A semi-infinite hole defect is present on the left side.

Therefore, we suppose this structure and the complete HgTe QW to have a similar edge state energy range $|E| < 1\ meV$.

Equilibrium case

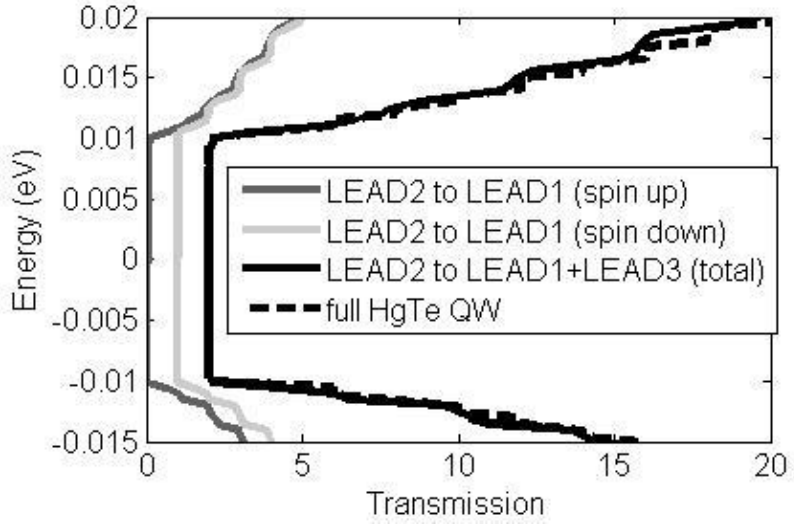

Figure 4.8: Transmission for equilibrium case. The fork-shaped HgTe QW (real block line), the transmission on LEAD1 (up and down for dark grey and light grey line), and the HgTe QW with the $width = 665\ nm$ without branch.(dashed line).

In figure 4.8, we compare the transmission for the fork-shaped HgTe QW and the complete HgTe QW strip. The semi-infinite defect decreases the transmission at the bulk states, but did not affect edge states transmission. We plotted the local transmission for LEAD2 to LEAD1 and showed that, at the edge state, only the spin down state allowed on LEAD1. This result is consistent with the fork-shpaed ZNR in figure 4.2.

Non-Equilibrium case

We then set the Fermi energy at $8.74\ meV$ to understand the behavior at the edge state; the applied small bias was set to $+0.002V_{ss}$, $-0.002V_{ss}$, and $+0.002V_{ss}$ on the LEADs 1, 2, and 3. The result of spin current polarization on LEAD1 was 0.957. In figure 4.9, the spin density accumulation demonstrates that this defect would not scatter the edge state electron. Conduction electrons occupied the edges such as in a complete HgTe QW. Conversely, few edge electrons move to the inner edges.

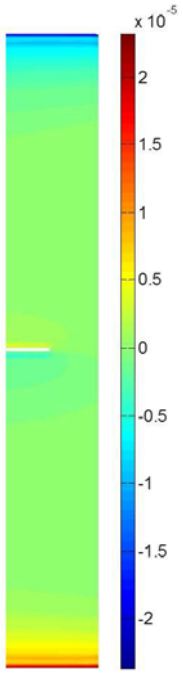

Figure 4.9: The spin density for the fork-shaped HgTe QW. The Fermi energy at $8.74\ meV$ and the bias voltage $eV = +(-)\,0.002V_{ss}$ on the right(left) side leads.

4.3.2 H-shaped HgTe/CdTe Quantum Well

The device consisted of $width = 665\ nm$ HgTe QW connected with four $width = 330\ nm$ HgTe QW. Several types of this geometry were present for N_L as shown in figure 4.10(b). Two arrangements were in this geometry: first, two semi-infinite holes on the left and right sides at $width = 665\ nm$ HgTe QW; and second, two HgTe QW with $width = 330\ nm$ were connected to each.

Equilibrium case

In the edge state region at $-1\ meV < E < 1\ meV$, the transmission of the spin down edge state mantain the quantized value 1 in figure 4.4. For spin up electron, we find the loss of quantized transmission at $0 < E < 0.01\ eV$. At $-1\ meV < E < 0\ meV$, the transmission close to zero in figure 4.4(a).

In figure 4.4(b), the transmission for the H-shaped ($L_x = 105\ nm$) HgTe QW was close to 2, and the local transmission (LEAD2'+4' to LEAD1') for spin up was close to zero.

It also appears that the transport property depends on the length for the rendezvous

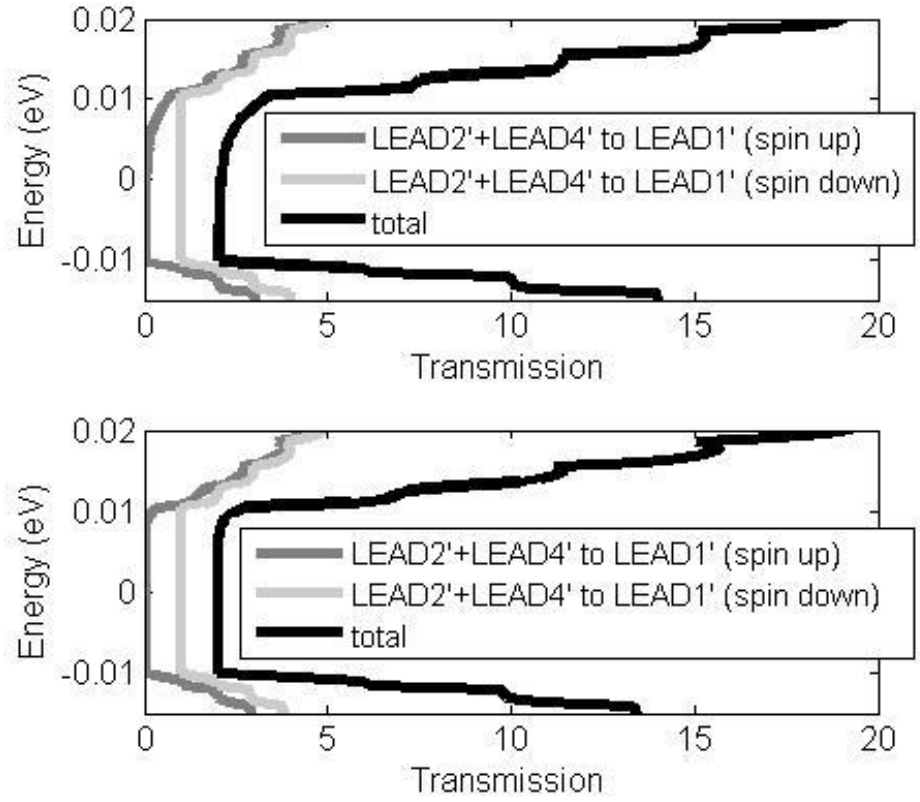

Figure 4.10: Transmission for the equilibrium case. The H-shaped HgTe QW (real block line) and transmission on LEAD1' (up and down for dark grey and light grey line) (a) $L_x = 45\ nm$ and (b) $L_x = 105\ nm$.

area.

Non-Equilibrium case

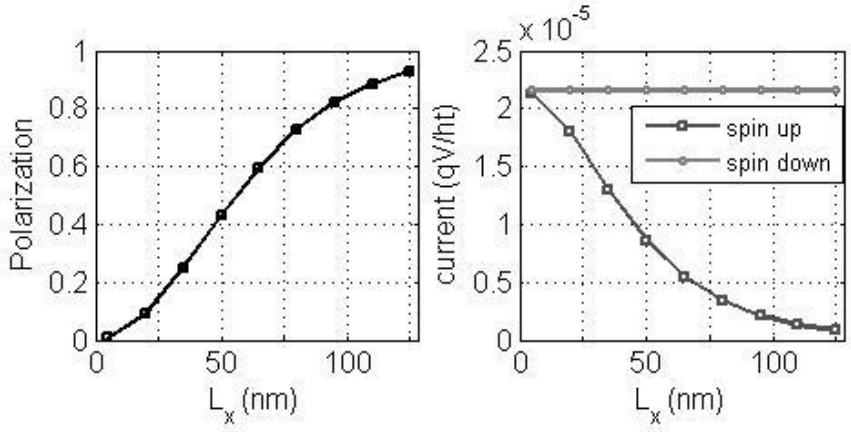

Figure 4.11: The spin current polarization (left) and current for spin up (dark grey) and down (light grey) (right) on LEAD1' with L_x.

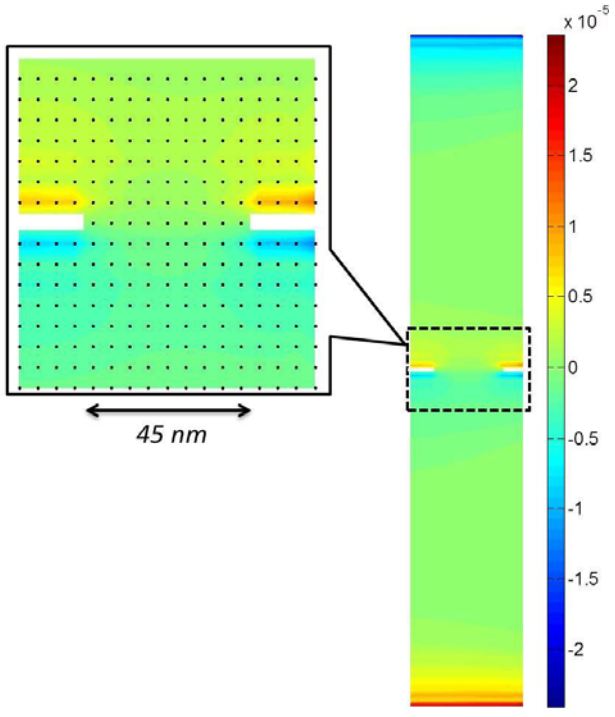

Figure 4.12: The spin density for the H-shaped ZNR. The Fermi energy at $8.7\ meV$ and the bias voltage $eV = +(-)\,0.002V_{ss}$ on the right (left) side leads. $L_x = 45\ nm$.

We then set the Fermi energy at $8.74\ meV$ to understand the behavior near the Dirac cone. The applied small bias was set at $eV = +0.002V_{ss}$ on LEAD2' and 4', then set $V = -0.002V_{ss}$ on LEAD1' and 3'.

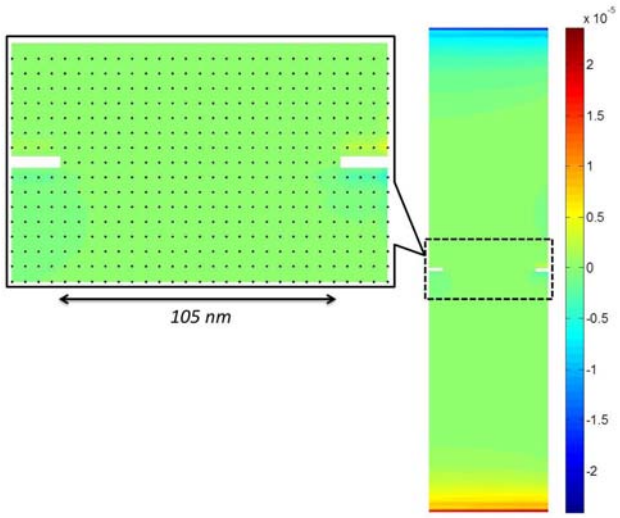

Figure 4.13: The spin density for the H-shaped ZNR. The Fermi energy at $8.7\ meV$ and the bias voltage $eV = +(-)\,0.002V_{ss}$ on the right (left) side leads. $L_x = 105\ nm$.

In figure 4.11, the spin down current on LEAD1' change with N_L. For $L_x = 105\ nm$, the spin down current the spin down current was close to 0, and the current polarization was close to 1. A number of local spin density areas were observed in the rendezvous region (see figure 4.12). However, for $L_x = 105\ nm$, the spin accumulation is few in the rendezvous region (see figure 4.13).

4.4 Discussion and Conclusion

In conclusion, the fork-shaped ZNR and the larger rendezvous region H-shaped ZNR both had a high spin polarization current on the branch channel. The smaller scattering region H-shaped ZNR would also gain the polarization current, but the polarization ratio depended on the size of the rendezvous region. In the future, we should take into account the Coulomb repulsion, disorder, and also larger size for a realistic system.

The difference quantity between ZNR and HgTe QW is the ratio of the fermi wavelength and rendezvous region length. The fermi wavelength of ZNR is $\lambda_F \cong 1\ a$ [9], is smaller then rendezvous region length $N_L < 27$ ($length \cong 36.4\ a$) as we set. Therfore, the polarizaion (and spin up current) was attenuating in an oscillatory manner with increasing the length of rendezvous region N_L; The fermi wavelength of HgTe QW is $\lambda_F \cong 992\ nm$, is larger then rendezvous region length $L_x < 125\ nm$ as we set. So, the

polarizaion (and spin up current) do not oscillate with increasing the length of rendezvous region L_x.

Our study provides an ideal view of the spin transport on "2D branch-shaped topological insulator". The inner branches of graphene nano-ribbon usually can enhance the spin polarization for both H-shape and fork shape.

Bibliography

[1] T. Ouyang, Y. Chen, Y. Xie, X. L. Wei, K. Yang, P. Yang, and J. Zhong, Phys. Rev. B **8**2, 245403 (2010).

[2] A. Jacobsen, I. Shorubalko, L. Maag, U. Sennhauser, and K. Ensslin, Appl. Phys. Lett. **9**7, 032110 (2010).

[3] Havard Haugen, Daniel Huertas-Hernando, and Arne Brataas, Phys. Rev. B **8**1, 174523 (2010).

[4] A. N. Andriotis and M. Menon, Appl. Phys. Lett. **9**2, 042115 (2008). Press, Cambridge, 1995). Press, Cambridge, 2005). 035412 (2002). (2006). 033715 (2010). Phys. **1**09, 07C721 (2011).

[5] D. Gosabez-Martez, J. J. Palacios, and J. Fernadez-Rossier. Phys. Rev. B **8**3, 115436 (2011).

[6] Z. Wang, N. Hao, and P. Zhang, Phys. Rev. B **8**0, 115420 (2009).

[7] F. Zhang, J. Jung, G. A. Fiete, Q. Niu, and A. H. MacDonald, Phys. Rev. Lett. **1**06, 156801 (2011).

[8] M. Konig, S. Wiedmann, C. Brune, A. Roth, H. Buhmann, L. W. Molenkamp, X. L. Qi, and S. C. Zhang, Science **3**18, 766 (2007).

[9] A. Isacsson, Phys. Rev. B **8**4, 125452 (2011).

Chapter 5

Impurity Influence in Quantum Spin Hall Transport

Influences of impurities on the electron density and transmission of a finite HgTe/CdTe quantum well sample are studied numerically in the framework of the Landauer-Buttiker formula. In a geometry of slab with finite width, electrons in helical edge states protected by the time-reversal symmetry can tunnel through non-magnetic impurities at two resonant energy levels. Electrons of one side can be scattered into the other side and the quantized conductance can be broken down. For a small sample with impurity, transmission coefficient can even drop to zero for the crosswalk between the helical edge states at two sample sides. Distance between helical edge states is critical for the suppression of the transmission. The s-orbital and p-orbital of pseudo-spins affect the quantized spin Hall current in a different way for their different energies.

5.1 Introduction

The CdTe/HgTe/CdTe system has a strong intrinsic spin-orbit interaction reported experimentally [2]. In a dirty system, for the protection of fundamental physical laws, the time reversal symmetry makes edge states robust against non-magnetic defect [3] [4], and weak interaction [5] [6]. The spin polarized electrons do not scatter backward by the defect for the time reversal symmetry and thus two-terminal conductivity of the electron

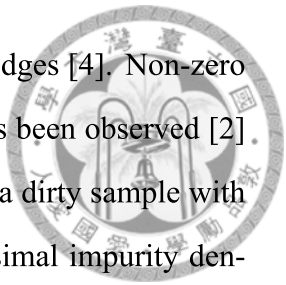

transmission is $2e^2/h$ for spin up and spin down branches along the edges [4]. Non-zero but not exactly quantized conductance in a band-insulating region has been observed [2] in HgTe/CdTe quantum well. The intrinsic spin Hall effect [7] [8] of a dirty sample with non-magnetic impurities has been intensive studied. For an infinitesimal impurity density of a dirty sample, the analytic calculations concluded a cancellation of the effect [9]. Numerical analysis of mesoscopic system with finite size [10] [11] [12] showed that the spin Hall effect persists up to a certain impurity density (the spin Hall current is produced by the spin-orbit interaction in two dimensional systems or semiconductors [13]). It was also reported that the quantum spin Hall phase can be completely destroyed due to the quantum percolation of the impurity bands within the gap of bulk bands and the localization-delocalization transition is accompanied by the vanishing of the quantum spin Hall phase [14]. However, detailed mechanism of delocalization and the non-quantization of spin Hall conductance remain unclear.

There are several possible paths which electrons of topological insulators with impurity can possibly go through. Two different kinds of path are shown in figure 5.1 and all possible paths obey the time reversal symmetry. The first one was discussed by Qi and Zhang [1] [2] [4]. In figure 5.1(b), electrons from edge states do not interact with impurity and the quantization of spin Hall conductance should be followed for this kind of electrons. Second possible path is that the electrons from edge state can interact with the impurity but cannot crosswalk with other branch of the edge. Therefore, it will tunnel in and out from the impurity, however, the time reversal symmetry requires that electrons of the helical edge state can move forward. For the second path in figure 5.1(c) electrons tunnel from edge states to bound states of impurity and back to the original edge states, there is a possibly phase shift induced from tunneling. Therefore, interference among figure 5.1(b) and figure 5.1(c) can reduce the spin Hall conductance and the reduction of transmission in figure 5.6(a) and figure 5.7(a) should be resulted from the interference of two different kinds of forward electrons. The third possible path in figure 5.1(d) is a tunneling path from one side to the other side of the sample edges, the time reversal symmetry requires the electrons to scatter backward of the same helical edge state.

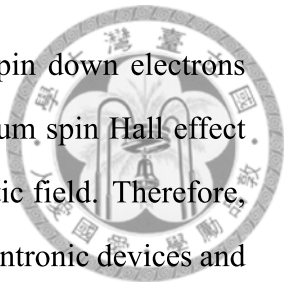

The robustness of quantum helical edge states of spin up and spin down electrons is useful for the new generation of nano-device. In particular, quantum spin Hall effect makes a topological insulator as a intrinsic spin filter without magnetic field. Therefore, the topological insulator enables several novel applications in both spintronic devices and quantum computers. Recent studies also reveal that Majorana fermions can exist possibly at the interface between topological insulators and superconductors with ferromagnetism. [15]. Nevertheless, transport measurement of the edge current is an important signature in the experiment. Until now most experimental evidences reported in 2D and 3D topological insulators are mostly focused only on energy spectrum [16] [17] [18] [19], and only a few experimental evidences are reported related to the transport of spin current [2]. Some analysis indicated that the impurities within topological insulator can induce a bound state near the helical edge states and thus affect the transport of the electron spins [14]. However, to the best knowledge of the authors, there is not a full non-equilibrium study on transport spin electrons within topological insulator, and neither is the impurity effect on the robustness of the quantized spin Hall conductance.

In this secion we applied the Green's function technique to study electron transport in the HgTe quantum well. A HgTe quantum well is a reported topological insulator with both edge energy dispersion and transport phenomenon [2]. In Chapter 2, we briefly introduce the Green's function method combined with tight-binding approaches to the 2D Hamiltonian of HgTe/CdTe quantum well [20]. We introduce a localized non-magnetic impurity to study the size effect of the 2D topological insulator in Sec. III. Two bound states of localized impurity are found from the superposition of s-orbital and p-orbital of electrons for either an attractive or a repulsive impurity potential. For a large size of HgTe/CdTe, the two branches of helical edge states at two sides of a sample act independently and also does not interact with localized impurity and the two-terminal conductance is always quantized to be $2e^2/h$. However, for a small size of HgTe/CdTe, even a single non-magnetic impurity affects the transport properties for the crosswalk between the upper branch and down branch of helical edge states. The bound state induced by the impurity provides a tunneling channel between the helical edge states on different sides. The

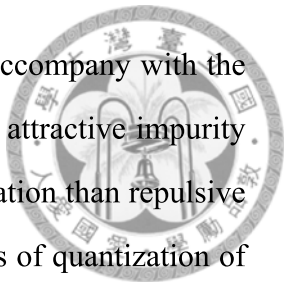

localization-delocalization transition at two resonance bound states accompany with the loss of quantization of the conductance. It is worth to point out that attractive impurity potential usually induces a more significantly influence on the dislocation than repulsive impurity potential. We conclude that our analysis that defect can loss of quantization of quantum spin Hall conductance via the crosswalk between helical edge states. Localized bound states with two bound energies of attractive and repulsive impunity potentials are identified. When the resonance tunneling between the helical edge states occurs, the non-quantization of the conductance can be observed.

In this study, we consider an infinite long sample (along x direction) of a finite width L_y with a nonmagnetic impurity of $5 \times 5nm^2$ located at $x = 0$. The position of the impurity along the y axis can be different: at the center of the sample, or closer to one of the side boundary. In the practical calculation, we divide the sample into three parts: the central part contains the impurity potential with a width L_x larger than the potential regime, and the left and right parts are regarded as two semi-infinite leads as introduced in Sec. IIB. After numerical calculations we found that the numerical results in the present study are insensitive to the values of L_x as anticipated, and thus we take $L_x = 15\ nm$ in the calculations. The Fermi energy is set to be $E_F = 0.00874\ eV$ at the Dirac cone of helical edge states if there is no specific indication.

We first plot the transmission with a series of different width L_y by means of the *Landauer-Biuttiker formalism* (equation 2.37), and decide the width for the further calculation in the absence of the impurity, i.e., $W = 0$. Then, we add a single non-magnetic impurity with dimension of $5 \times 5\ nm^2$ to the sample region. We decide the impurity affect by vary the impurity potential W in equation 5.1. In the calculation we take several specific values within the range of ($-0.5\ eV \leq W \leq 0.5$ eV) and show the non-trivial range in figure 5.4-5.7. Two samples with different dimensions are analyzed to study the size effect on the defect induced localization-delocalization transition. For simplicity we study two cases of $L_y = 2005\ nm$ and $295\ nm$, respectively. We also take into additional account the locations of the impurity. Two different situations are considered within all samples, a central defect between two edges and an edge defect near the upper edge [see

figure 5.2]. Two clear samples are also calculated for comparison. Thus direct tunneling between the helical edge states at two sides from the finite size effect and the indirect tunneling through the impurity can be easily distinguished.

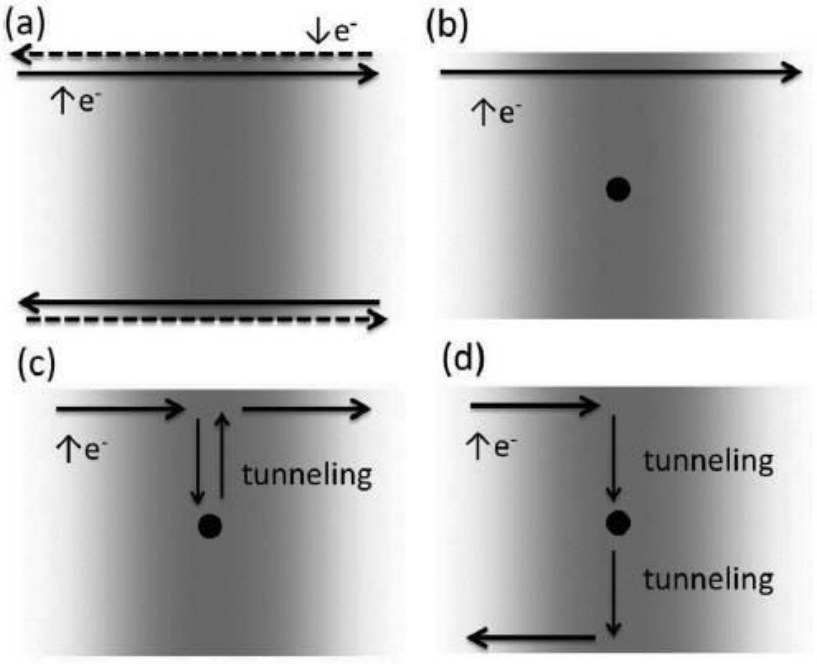

Figure 5.1: (a) Helical edge-state currents of the topological insulator.(b) The edge-state current does not interact with impurity.(c) The edge-state current tunnels to the impurity bound state and tunnels back to the original edge.(d) The edge-state current tunnels to the impurity bound state and tunnels to the opposite edge state. To clear the picture, we only show the one-channel spin-up electron path with impurity; the other channel and spin follow the symmetry path.(a),(b) $L_y = 2005\ nm$; (c),(d) $L_y = 295\ nm$.

5.2 Impurity Potentail Matrix in Tight-Binding Model

The impurity potential in a sample is introduced by including

$$W = \sum_i \varphi_i^\dagger \begin{bmatrix} W_i & 0 & 0 & 0 \\ 0 & W_i & 0 & 0 \\ 0 & 0 & W_i & 0 \\ 0 & 0 & 0 & W_i \end{bmatrix} \varphi_i \tag{5.1}$$

where $W_i = W$ is on the lattice site i in the potential area; otherwise, $W_i = 0$. In this paper, we only consider the upper block matrix for the two pseudo-spin-up states. The contributions from the states for the pseudo-spin-down states are their counterpartners of the upper block matrix under the time reversal.

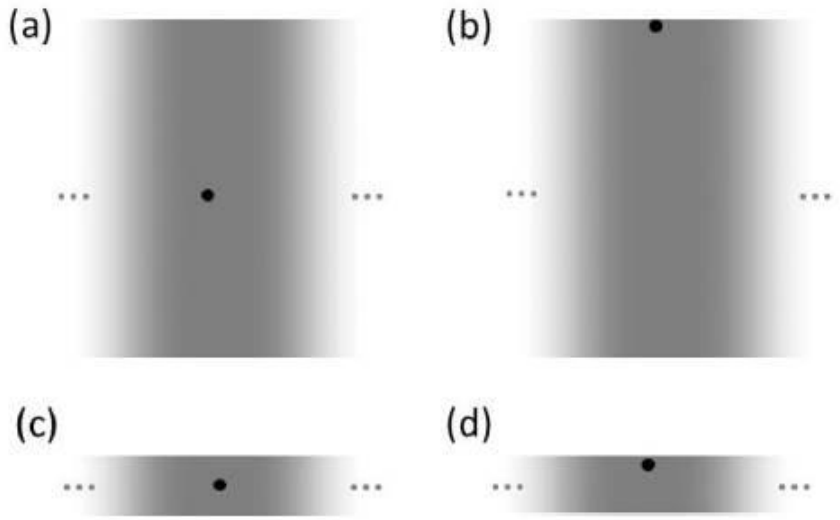

Figure 5.2: An impurity located in the HgTe quantum well sample.(a),(b) $L_y = 2005\ nm$; (c),(d) $L_y = 295\ nm$.

5.2.1 Clear Limit of Two Samples

We first study two samples without the impurity. Here we studied several different widths to understand the size effect in the clean case and we did not observe loss of quantization spin Hall conductance until the width less than $120\ nm$ as shown in figure 5.3a. A sharp transition from one to zero in the clean limit for narrow width sample, which is expected as the finite size effect [22]. In this calculation the Fermi level is fixed at $E_F = 8.47\ meV$. If we we plot the transmission coefficient as a function of the Fermi energy, it is observed that the transmission coefficient drops to zero at a finite range near $E_F = 7.5$ meV for $L_y = 295\ nm$ and $120\ nm$ as shown in figure 5.3b. This demonstrates an energy gap opening near the crossing point of energy dispersion of helical edge states.

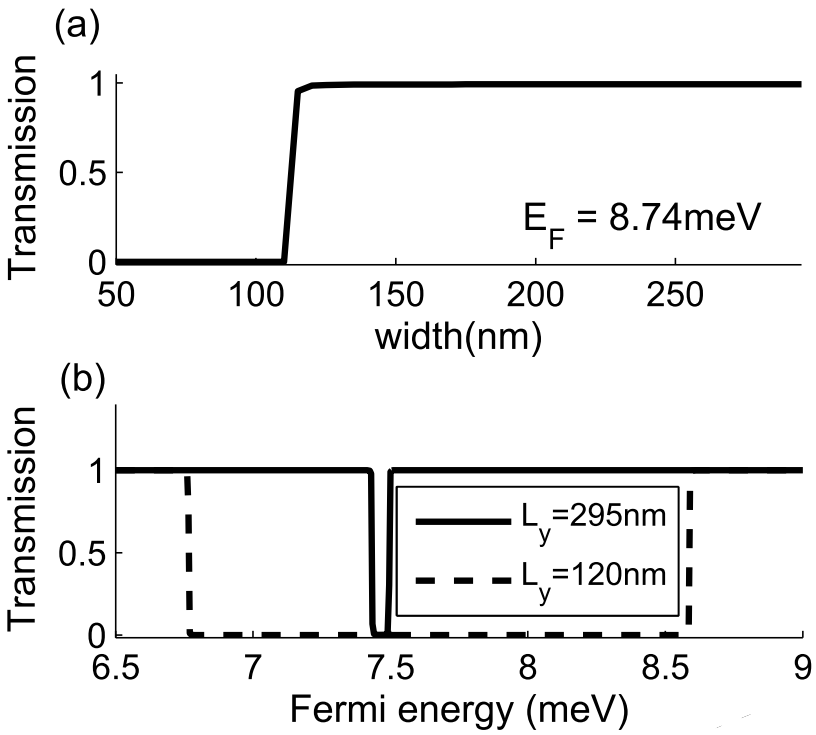

Figure 5.3: (a) The transmission coefficient as a function of the sample width for the Fermi energy is $E_F = 8.74\ meV$.(b) The transmission coefficient as a function of the Fermi energy E_F for $L_y = 295\ nm$ and 120nm.

5.3 In-gap Bound States Induced by Impurity

In the calculation, we found the formation of two in-gap bound states induced by the impurity. The two bound states have positive and negative energies, respectively.

For an attractive impurity potential of $W = -439.2\ meV$, electrons are in favor to jump into the defect region. The bound state energy is $E_- = -439.2\ meV$ for the impurity in the center [figure 5.3(a) and 5.3(c)] and $E_- = -328.5\ meV$ for the impurity on the edge[figure 5.3(b) and 5.3(d)]. $|s,\uparrow\rangle$ electrons will form an isotropic and circularly in-gap bound state near the defect site, while $|p_x + ip_y,\uparrow\rangle$ electrons are form a ring structure outside the $|s,\uparrow\rangle$ electrons circle. The low energy $|s,\uparrow\rangle$ is within the quantum well while the $|p_x + ip_y,\uparrow\rangle$ electrons are circulating around the potential well [figure 5.4(b), 5.4(d), 5.5(b), 5.5(d), 5.6(c), 5.6(e), 5.7(c) and 5.7(e)].

For a repulsive impurity potential of $W = +72.2\ meV$, a new boundary is formed to attract electrons surrounding around as the formation of the edge states near the boundary. The bound state energy $E_+ = 0.0722\ eV\ , 0.0516\ eV, 0.0719\ eV, 0.0516\ eV$ for

figure 5.3(a)-(d)), respectively. $|p_x + ip_y, \uparrow\rangle$ electrons form a in-gap bound state with circular distribution within defect while the low energy $|s, \uparrow\rangle$ electrons accumulates as a ring-like structure outside defect[figure 5.4(c), 5.4(e), 5.5(c), 5.5(e), 5.6(d), 5.6(f), 5.7(d) and 5.7(f)]. Although the spatial distributions of $|p_x + ip_y, \uparrow\rangle$ and $|s, \uparrow\rangle$ are very different in the in-gap bound states with positive and negative energy, $|p_x + ip_y, \uparrow\rangle$ and$|s, \uparrow\rangle$ electrons resonate at the same energy. Similar phenomenon was reported for various dimensions of topological insulator including HgTe quantum well in continuous model [23].

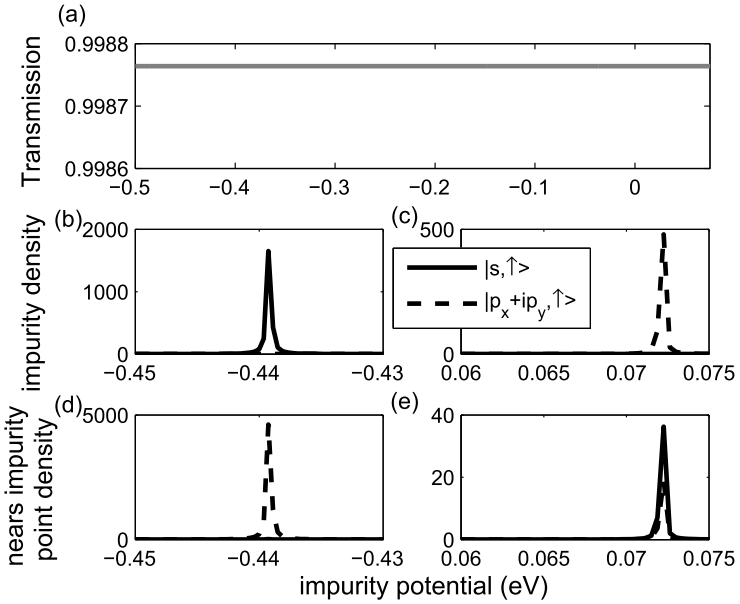

Figure 5.4: $L_y = 2005\ nm$, the impurity in the center of the slab ($y = 0$).(a) The transmission coefficient of topological insulator with the impurity is the same with different amplitude W of the impurity potential.(b) The charge density on the impurity site with an attractive potential ($W < 0$).(c) The charge density on the impurity site with a positive potential ($W > 0$).(d) The charge density around the impurity site with attractive potential ($W < 0$).(e) The charge density around the impurity site with a positive potential ($W > 0$).

5.4 Discussions and Conclusions

Our studies indicate that even though the helical edge states are robust against small nonmagnetic impurity from the protection of time-reversal symmetry, the quantized spin Hall conductance is quite sensitive to the impurity in a finite-size sample. Transmission of the robust helical states can be reduced from the crosswalk between helical edge states at

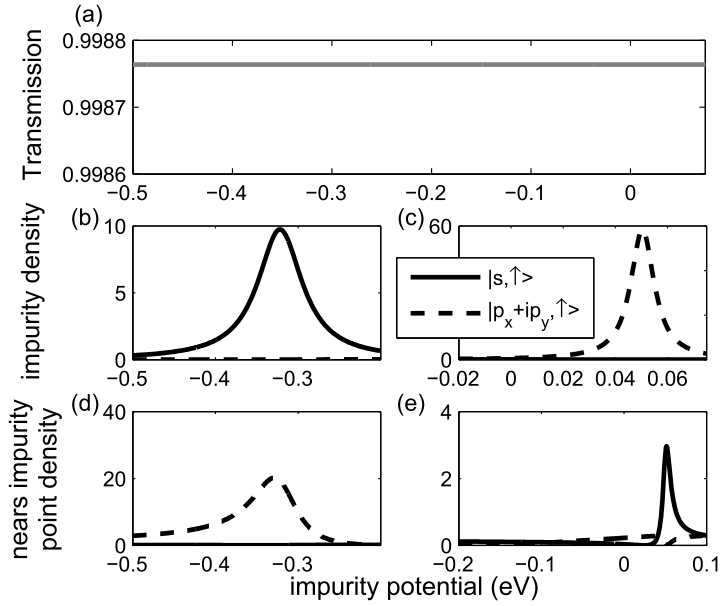

Figure 5.5: $L_y = 2005\ nm$, the impurity located on the edge ($y = 1000\ nm$).(a) The transmission coefficient of topological insulator with the impurity is the same with different amplitude W of the impurity potential.(b) The charge density on the impurity site with an attractive potential ($W < 0$).(c) The charge density on the impurity site with a positive potential ($W > 0$).(d) The charge density around the impurity site with attractive potential ($W < 0$).(e) The charge density around the impurity site with a positive potential ($W > 0$).

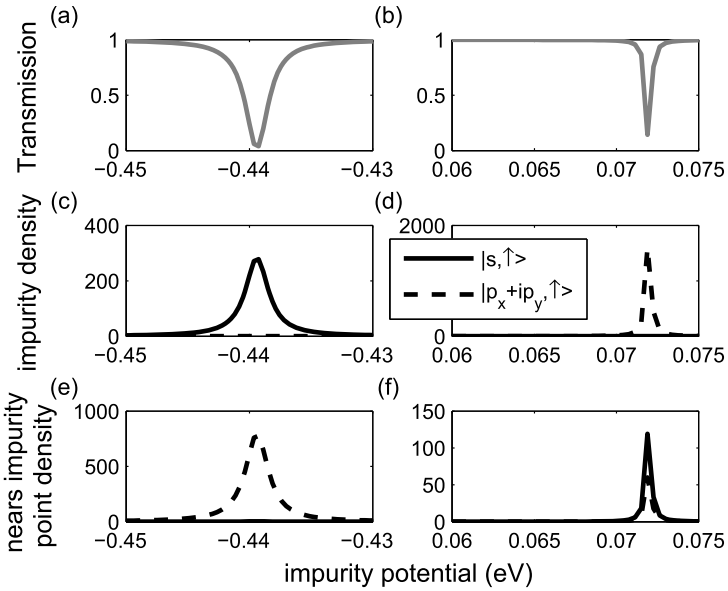

Figure 5.6: $L_y = 295\ nm$, the impurity located in the center ($y = 0$).(a)-(b) The transmission coefficient of topological insulator with the impurity is the same with different amplitude W of the impurity potential.(c) The charge density on the impurity site with an attractive potential ($W < 0$).(d) The charge density on the impurity site with a positive potential ($W > 0$).(e) The charge density around the impurity site with attractive potential ($W < 0$).(f) The charge density around the impurity site with a positive potential ($W > 0$).

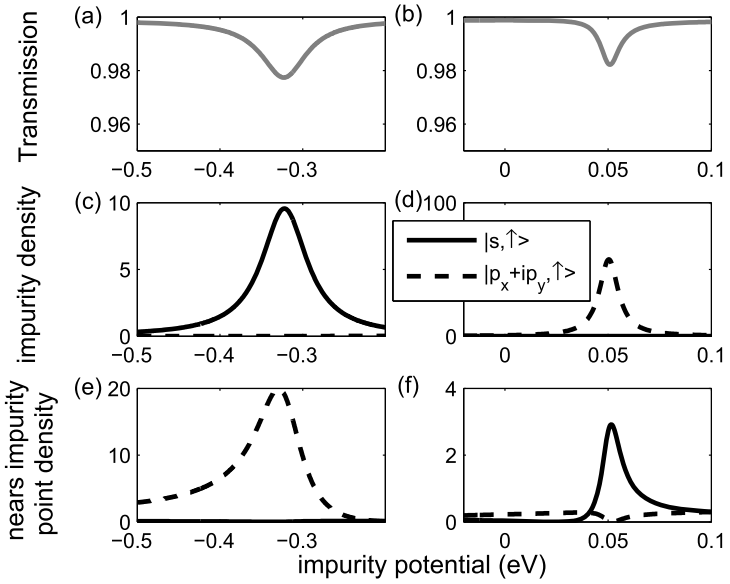

Figure 5.7: $L_y = 295\ nm$, the impurity located on edge ($y = 145\ nm$).(a)-(b) The transmission coefficient of topological insulator with the impurity is the same with different amplitude W of the impurity potential.(c) The charge density on the impurity site with an attractive potential ($W < 0$).(d) The charge density on the impurity site with a positive potential ($W > 0$).(e) The charge density around the impurity site with attractive potential ($W < 0$).(f) The charge density around the impurity site with a positive potential ($W > 0$).

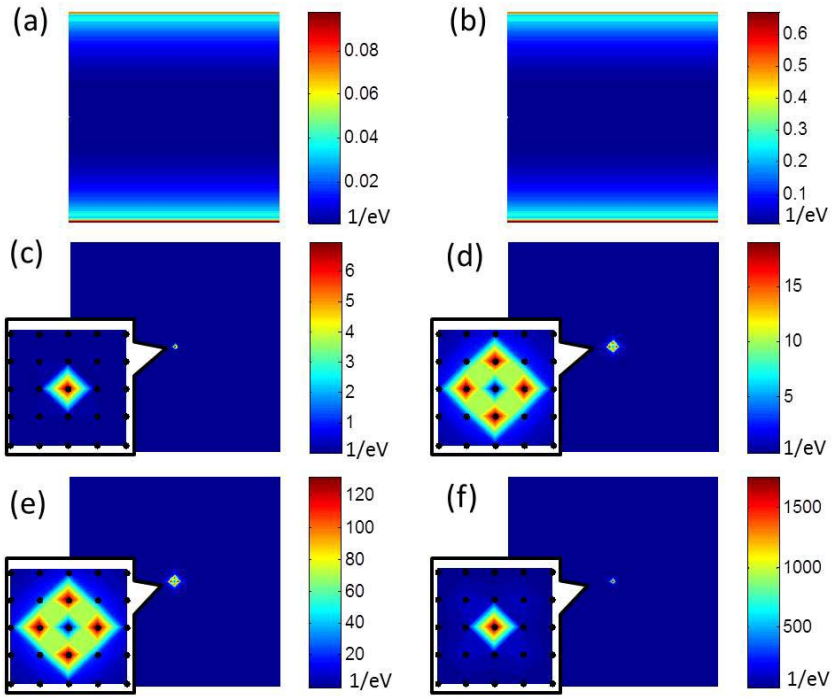

Figure 5.8: The local density of state for the $L_y = 295\ nm$ HgTe QW, $E_F = 8.74\ meV$. (a) $|s,\uparrow\rangle$ state in a clear system.(b) $|p_x + ip_y,\uparrow\rangle$ state in a clear system.(c) $|s,\uparrow\rangle$ state at $W = -439.2\ meV$.(d) $|p_x + ip_y,\uparrow\rangle$ state at $W = 71.9\ meV$.(e) $|s,\uparrow\rangle$ state at $W = -439.2\ meV$.(f) $|p_x + ip_y,\uparrow\rangle$ state at $W = 71.9\ meV$.

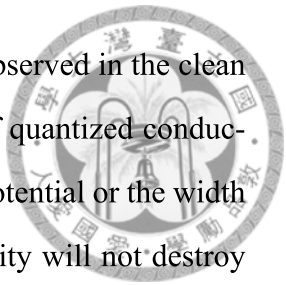

two sides. The finite-size effect of topological insulator is not only observed in the clean case, but also is significant with impurity inside the sample. Loss of quantized conductance of edge electrons depends on either the amplitude of impurity potential or the width of the sample. From our analysis, we know that nonmagnetic impurity will not destroy the helical edge states but it will induce tunneling between two helical edge states. The finite-size effect can open an energy gap on the helical edge state and direct overlapping of wave function from two helical edge states, which may let the nondissipative conducting quantum spin Hall channel disappear. Another possible reduction mechanism of quantized spin Hall conductance is from the impurity within topological insulator; impurity-induced bound states provide a crosswalk channel of helical edge states. In summary, for a quantum spin Hall nanodevice, the impurity in a 2D CdTe/HgTe/CdTe system of topological insulators can change the electronic structure and also the transport features within sample. The electrons within the helical edge states can trasverse through impurity and crosswalk to other branches and this transition induces the reduction of quantization spin Hall conductance.

Bibliography

[1] B. A. Bernevig, T. L. Hughes, and S. C. Zhang, Science, **314**, 5806 (2006) .

[2] M. Konig, S. Wiedmann, C. Brune, A. Roth, H. Buhmann, L. W. Molenkamp, X. L. Qi, and S. C. Zhang, Science **318**, 766 (2007).

[3] C. L. Kane and E. J. Mele, Phys. Rev. Lett. **95**, 146802 (2005).

[4] X. L. Qi and S. C. Zhang, Phys. Today **63(1)**, 33 (2010).

[5] C. Wu, B. A. Bernevig, and S. C. Zhang, Phys. Rev. Lett. **96**, 106401 (2006).

[6] C. Xu and J. E. Moore, Phys. Rev. B **73**, 045322 (2006).

[7] J. Schliemann, and D. Loss, Phys. Rev. B **69,** 165315 (2004).

[8] J. Sinova, S. Murakami, S.Q. Shen, and M. S. Choi, Solid State Commun. **138**, 4 (2006).

[9] Ol'ga V. Dimitrova, Phys. Rev. B **71,** 245327 (2005).

[10] N. Sugimoto, S. Onoda, S. Murakami, and N. Nagaosa, Phys. Rev. B **73,** 113305 (2006).

[11] C. P. Moca and D. C. Marinescu, Phys. Rev. B **72,** 165335 (2005).

[12] B. K. Nikolić, S. Souma, L. Zârbo, and J. Sinova, Phys. Rev, Lett. **95,** 046601 (2005).

[13] B. A. Bernevig, J. Hu , E. Mukamel, and S. C. Zhang, Phys. Rev. B **70,** 113301 (2004); B. A. Bernevig and S. C. Zhang, Phys. Rev. B **72,** 115204 (2005); E. I.

Rashba, Phys. Rev. B **68,** 241315 (2003); A. A. Burkov, A.S. Nunez, and A. H. MacDonald, Phys. Rev. B **70,** 155308 (2004).

[14] R. L. Chu, J. Lu, and S. Q. Shen. EPL, **100**, 17013 (2012).

[15] L. Fu and C. L. Kane, Phys. Rev. Lett. **100**, 096407 (2008).

[16] D. Hsieh, D. Qian, L. Wray, Y. Xia, Y. S. Hor, R. J. Cava .and M. Z. Hasan, Nature **452**, 970 (2008).

[17] D. Hsieh, Y. Xia, D. Qian, L. Wray, J. H. Dil, F. Meier, J. Osterwalder, L. Patthey, J. G. Checkelsky, N. P. Ong, A. V. Fedorov, H. Lin, A. Bansil, D. Grauer, Y. S. Hor, R. J. Cava, and M. Z. Hasan, Nature **460**, 1101 (2009).

[18] X. Dai1, T. L. Hughes, X. L. Qi, Z. Fang, and S. C. Zhang, Phys. Rev. B **77**, 125319 (2008).

[19] Y. L. Chen, J. G. Analytis, J. H. Chu, Z. K. Liu, S.K. Mo, X. L. Qi, H. J. Zhang, D. H. Lu, X. Dai, Z. Fang, S. C. Zhang, I. R. Fisher, Z. Hussain, Z. X. Shen, Science **325**, 178 (2009).

Cambridge University Press, Cambridge (2005).

[20] H. Jiang, L. Wang, Q. F. Sun, and X. C. Xie, Phys. Rev. B **80**, 165316 (2009).

[21] M. P. Lopez Sancho, J. M. Lopez Sancho, J. M. L. Sancho, and J. Rubio, J. Phys. F: Met. Phys. **15,** 851 (1985).

[22] B. Zhou, H. Z. Lu, R. L. Chu, S. Q. Shen, and Q. Niu. Phys, Rev. Lett. **101**, 246807 (2008).

[23] J. Lu, W. Y. Shan, H. Z. Lu, and S. Q. Shen, New J. Phys. **13** (2011).

[24] D. J. Thouless, M. Kohmoto, M. P. Nightingale, and M. Nijs, Phys. Rev. Lett. **49**, 405 (1982).

Chapter 6

The impurity in H-shaped Topological Insulator Device

6.1 Introduction

In Chapter 5, we have shown the localized bound state of an impurity affect the transport property in the finite width topological insulator by the quantum tunneling. It inspire us to design a device that can display this effect. That is a H-shaped geometry of the 2D topological insulator as figure 6.1, the sample connect with four leads that are the same materials, and the non-magnetic impurity is added in the center of the sample. In this study, we chose HgTe/CdTd quantum well as the sample because that is a reported 2D topological insulator with both edge energy dispersion and transport phenomenon [1].

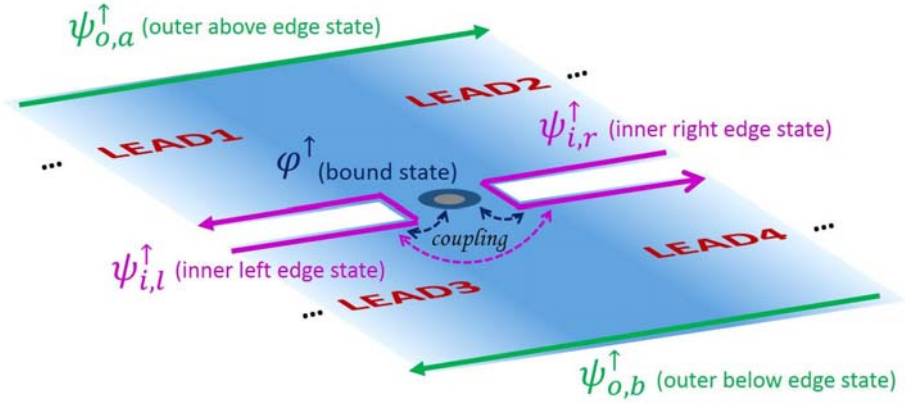

Figure 6.1: Four edge states and the localized bound state.

In this model, the fermi energy intersect the edge state $E_f = 8.74\ meV$, we have four edge sates, outer above(and below) and inner left(and right), there is the localized bound state at appropriate impurity potential values as figure 6.1.

This geometry have a different electron path with the sample case (figure 5.2). In figure 6.2, the electron moving from the inner left edge state, there are four possible path in this situation.

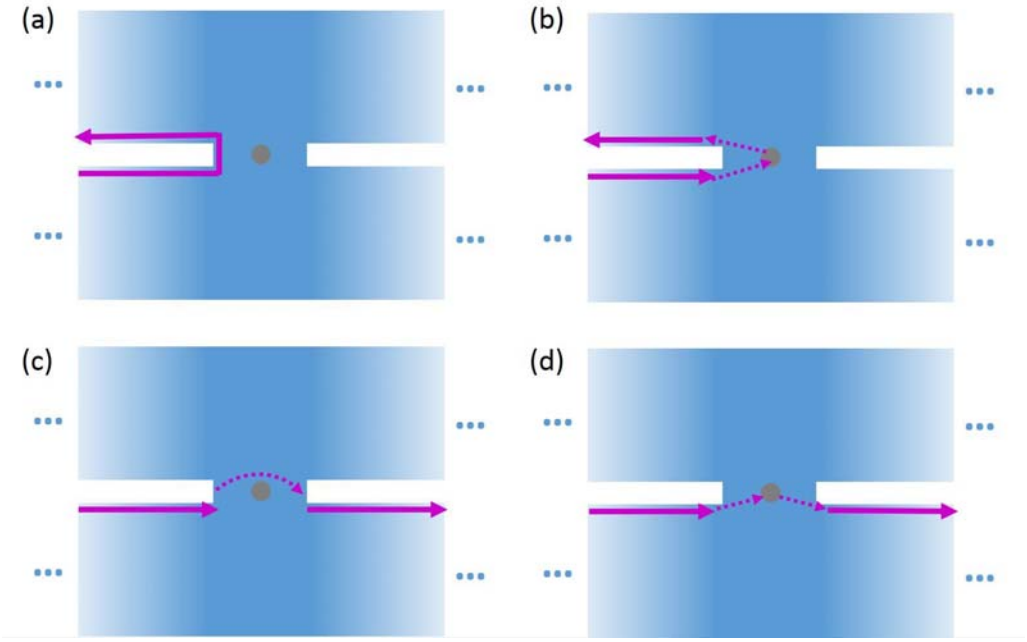

Figure 6.2: The different electron paths from the inner left edge.(a) The edge state electron does not interact with the impurity, and moves on the same edge. (b)The edge state electron tunnels to the impurity bound state and tunnels back to the original edge. (c) The edge state electron does not interact with the impurity, but tunnels to the inner right edge. (d) Thee edge state electron tunnels to the inner right edge through the impurity bound state.

In this study, the transmission is plotted by *Landauer-Biuttiker formalism* (equation 2.37). And the tight-binding Hamiltonian of the HgTe is bulding in section 3.3.2, the impurity potential is introduced by 5.2. Because the spin up and down are symmetry, so we only consider the pseudo spin up state like Chapter 5.

6.2 Clear Limit of Device

We first study the clean sample without an impurity. To know the relation between the electron path and the geometry, we vary the length of rendezvous region L_x then the dis-

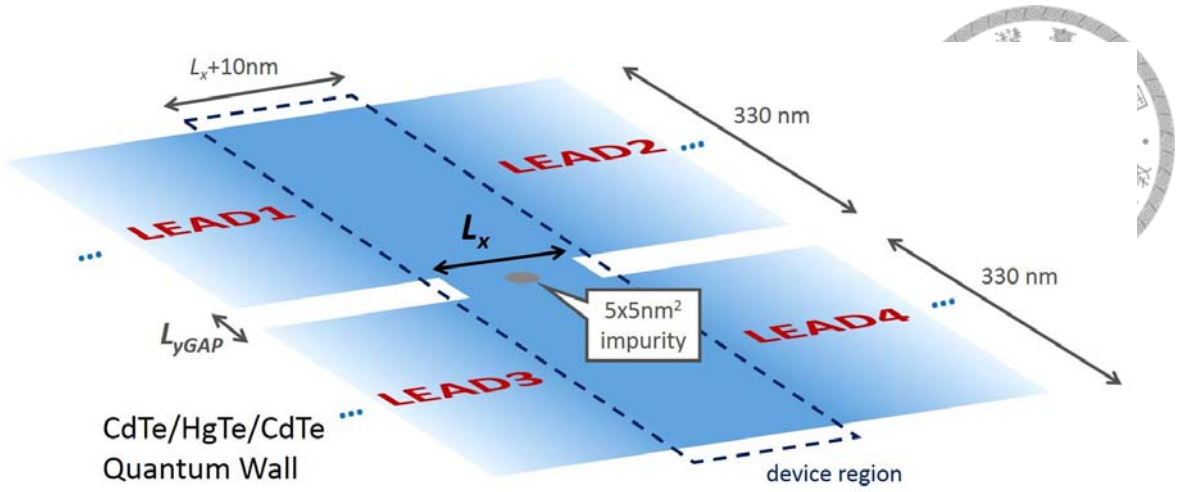

Figure 6.3: The impurity in the H-shaped HgTe/CdTe quantum well with four leads.

tance are $L_{yGAP} = 5\ nm$ and $L_{yGAP} = 15\ nm$,and plot the inner edge state transmission form LEAD3 to LEAD4 in figure 6.4.

The transmission of $L_{yGAP} = 5\ nm$ is higher than $L_{yGAP} = 15\ nm$, because long L_{yGAP} provide the more opportunities for contact. And the transmission between two inner edge states is depend on the length of the rendezvous region L_x, because the coupling strength of two inner edge states (left and right) change with the distance of two edges.

Two inner edge states are coupling each other in the appropriate value of L_{yGAP} and L_x. So the path is possible in figure 6.2(c) without an impurity bound state.

6.3 Impurity Bound State and Interference Resonance

We vary the impurity potential and plot the transmission with two different width $L_x = 45\ nm$, $105\ nm$ in figure 6.5 . The data show that the transmission of LEAD3 to LEAD1 and LEAD3 to LEAD4 are complementary, so this result indicate that the electron do not scatter back to the source lead. When $L_x = 45\ nm$, we found the interesting resonance at two impurity potential values. The transmission "LEAD3 to LEAD4" not only enhance but reduce in two resonance regions. This phenomenon is correspond to the "Fano resonance" [2] [3] that is the quantum interference of a discretized state and continuum state. Two paths (as figure 6.2(c), (d))

The structure of $L_x = 105\ nm$ case have the same behavior, but the resonance become

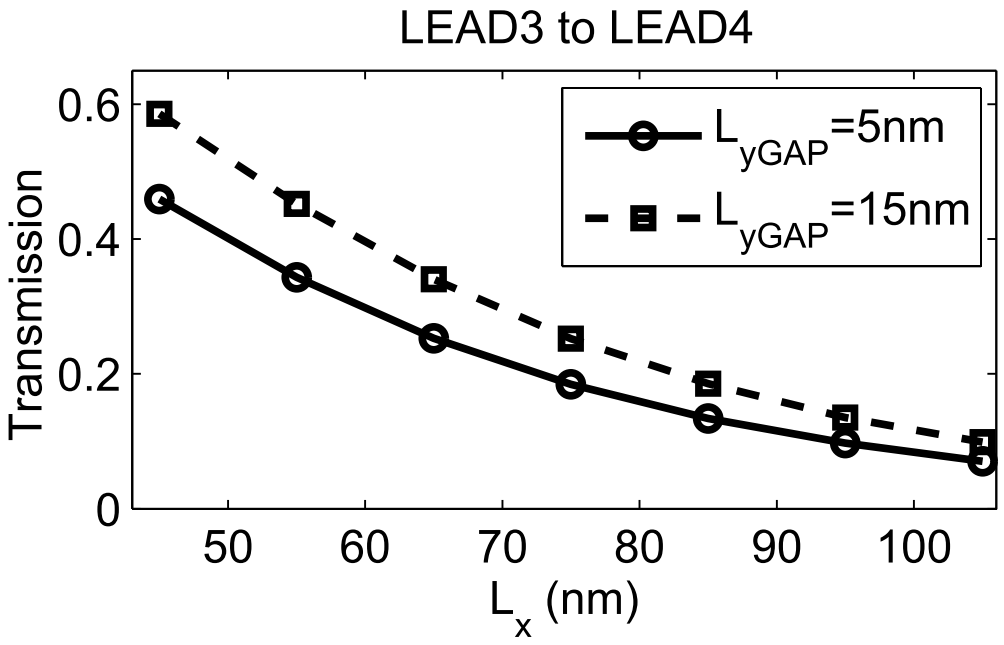

Figure 6.4: In the clean case, the transmission form LEAD3 to LEAD4 and the length of the rendezvous region L_x, $L_{yGAP} = 5\ nm$ (for the real line), $15\ nm$ (for the dash line).

sharp because the distance between the discretized impurity bound state and edge state is longer than the structure of $L_x = 45\ nm$.

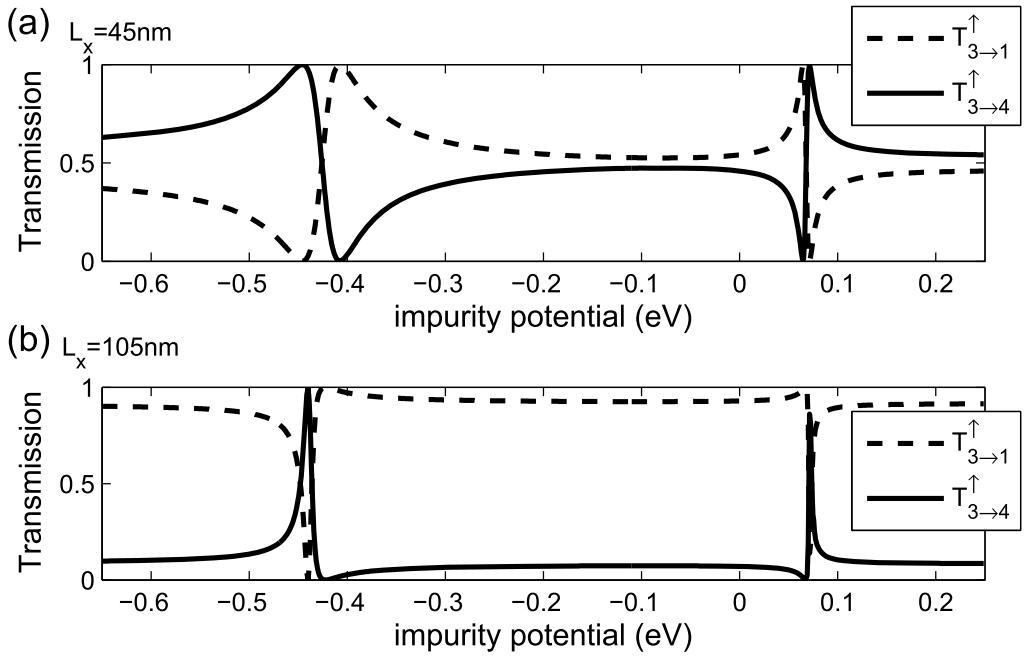

Figure 6.5: The impurity potential vs Transmission, (a) $L_x = 45\ nm$, (b) $105\ nm$

6.4 Discussions and Conclusions

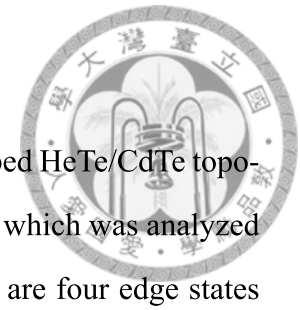

In this chapter, we put a non-magnetic impurity within the H-shaped HeTe/CdTe topological insulator to study the interplay of the impurity and edge state which was analyzed in Chapter 5. In our H-shaped structure topological insulator, there are four edge states including two outer edges and two inner edge states of H-shaped topological insulator. We arbitrarily choose a dimension of H-shaped insulator which two inner edge states will tunnel without impurity and the outer edge states are rather far without the significant crosswalk to inner edge states. A finite transmission of H-shaped structure without the impurity indicates the tunneling of spin electrons within the edge states. Moreover, rendezvous region within the H-shaped structure influences the overlapping of edge states and thus the transmission. For the dimension size which we studied, the outer edge states are rather far comparing with the inner edge states and thus only the inner edge states will interact with the impurity. It means that the transmission of H-shaped topological insulator only depends on the inner edge states instead of the outer edge states.

With the impurity, the transmission of LEAD1 and LEAD4 of H-shaped structure (figure 6.5) are complementary and the sum of these two transmission is always unit for the conservation of electrons within this system. The time reversal symmetry is still conserved within the edge states. With the variation of on-site impurity potential, the electron of one edge state can be resonant tunneling into the other edge state, the transmission of LEAD1 will shut down and the LEAD4 will open. This crosswalk phenomenon among the edge states through the resonant tunneling of impurity bound states is indeed the same physics as we described in Chapter 5.

Moreover, the interplay among edge states and impurity bound state can also induce a destructive interference where an interference among the direct tunneling of edge states and the tunneling through impurity bound states. It means that the electrons thus cannot travel from one side of H-shaped to the other side at all. However the backward transmission through the initial edge will then be constructive interference and the transmission is 1. The spectral of transmission is from the competition between of quantum tunneling and quantum interference. Here the spectral of transmission is just a Fano resonance

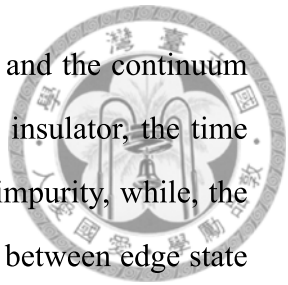

from the competition between discrete state of impurity bound state and the continuum state of edge state. In summary, the H-shaped structure topological insulator, the time reversal symmetry protect the backward scattering of non-magnetic impurity, while, the quantum tunneling among edges states and the quantum interference between edge state and impurity bound state can still significantly influence the transmission of the topological insulator device. It also suggested that the analysis of the transmission of topological insulator nano device should be more carefully analyzed for the transmission robustness. In conclusion, we are not only identifying the quantum tunneling among edge states but also observe the quantum interference among the bound state and edge states. We can use the quantum tunneling and interference to make a rather robust topological insulator nano device. The impurity within the H-shaped structure can be manipulated by a gate voltage.

Bibliography

[1] M. Konig, S. Wiedmann, C. Brune, A. Roth, H. Buhmann, L. W. Molenkamp, X. L. Qi, and S. C. Zhang, Science **3**18, 766 (2007).

[2] U. Fano, Phys. Rev. **1**24, 1866 (1961).

[3] Andrey E. Miroshnichenko, Sergej Flach, and Yuri S. Kivshar. Rev. Mod. Phys. **8**2, 2257

Chapter 7

Summary and Outlook

7.1 Summary

In this dissertation, we consider the topological insulator material in two realistic situations. First is the geometry effect, the geometry affect the spin polarization on the applied bias. The fork-shaped TI and the larger scattering region H-shaped TI both had a high spin polarization current on the branch channel. The smaller scattering region H-shaped TI would also gain the polarization current, but the polarization ratio depended on the size of the scattering region.

The second, we shown that the impurity in a 2D CdTe/HgTe/CdTe system of topological insulators can change the electronic structure and also the transport features within sample. The electrons within the helical edge states can trasverse through impurity and crosswalk to other branches and this transition induces the reduction of quantization spin Hall conductance. So the width of the sample and the concentration of the impurity density should be considered in the application.

After the test of the realistic case, we design the H-shaped device and the non-magnetic impurity is added in the center of the sample. In this system, the time reversal symmetry protect the backward scattering of non-magnetic impurity, while, the quantum tunneling among edges states and the quantum interference between edge state and impurity bound state can still significantly influence the transmission of the topological insulator device. It also suggested that the analysis of the transmission of topological insulator nano device

should be more carefully analyzed for the transmission robustness. This phenomenon shown that the direction of the electron current can be manipulated by the gate voltage, it is potential to be a switch in the electric circuit.

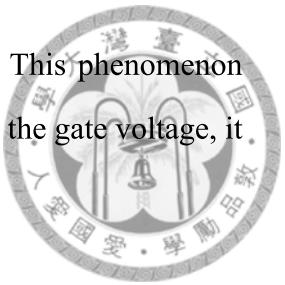

7.2 Outlook

All of the studies of dissertation are focus on the time-independent stable state, however, recently are shown the time-periodic system such as the AC bias and electromagnetic wave [1] [2]. The other potentail topic is the magnetic impurity, it can break the time-reversal symmetry and let the spin up and down exist defferent behavior [3]. For the realistic system, we can take into account the Coulomb repulsion, disorder, and also larger size.

Bibliography

[1] Netanel H. Lindner, Gil Refael and Victor Galitski. Nature Physics 7, 490–495 (2011)

[2] Mikael C. Rechtsman, Julia M. Zeuner, Yonatan Plotnik, Yaakov Lumer, Daniel Podolsky, Felix Dreisow, Stefan Nolte, Mordechai Segev and Alexander Szameit. Nature 496, 196–200 (2013)

[3] Qin Liu, Chao-Xing Liu, Cenke Xu, Xiao-Liang Qi, and Shou-Cheng Zhang. Phys. Rev. Lett. 102, 156603 (2009)